CHAPTER – 4

AA 6082 Al-alloy based Metal Matrix Composite Reinforced with Al-Cu-Fe Quasicrystal

CHAPTER 4

AA 6082 Al-alloy based Metal Matrix Composite Reinforced with Al-Cu-Fe Quasicrystal

The present chapter deals with the synthesis of Al-Cu-Fe reinforced AA6082 Al matrix nanocomposites through mechanical milling (MM) followed by its consolidation by spark plasma sintering (SPS). Previous studies have reported the synthesis of Al-IQC composite through liquid metallurgy and powder metallurgical processing. The retention of IQC after sintering of Al-IQC phase is still challenging to the scientific community. In an investigation Ali et al. [319] reported the formation Al-IQC compsite through hot-pressing and illustrated the effect of hot extrusion temperature on the phases formed. Further, it was also observed by Laplanche et al. [382] that Al-IQC composite prepared by hot isostatic pressing at 623 K are inferior to Al-ω (Al_7Cu_2Fe) composite fabricated at 823 K. The AA 6082 Al alloys are the candidate structural material for automotive applications and its may offer better microstructural features with enhanced mechanical properties.

In the present investigation, efforts were made to study the structural, morphological and phase composition of age-hardenable AA 6082 Al matrix composite reinforced with Al-Cu-Fe IQC through high energy ball milling (HEBM). The structural information, morphological features and phase composition were ascertained through XRD and TEM, and SEM respectively. Fabrication of these Al-IQC composite through spark plasma sintering (SPS) at different temperature gives us insight into microstructural evolution by formation of various phase during sintering and its interface with the Al based matrix. For fabricating Al – IQC composite without any significant fraction of ω-Al_7Cu_2Fe phase, efforts were also made to consolidate them through SPS at high pressure moderate temperature. The structure, microstructure and mechanical properties of Al–IQC composites fabricated at high pressure and moderate temperature were studied

systematically. The SPSed Al-IQC composite has appreciable mechanical properties due to interfacial strengthening.

4.1 Phase analysis of mechanically milled Al–IQC nanocomposite powder

4.1.2 XRD analysis of Al-IQC nanocomposite powder

The Figure 4.1 (a) shows powder XRD pattern of FCC-Al having all major reflections i.e. (111), (200), (220), (311) and (222). Figure 4.1 (b) shows the powder XRD pattern corresponding to face-centred ordered Al-Cu-Fe IQC phase having minor amount of crystalline phases, i.e. $Al_{13}Fe_4$ (a=1.549 nm, b=0.808 nm, c=1.248 nm, α=β=90˚, γ=107.720˚; mC102; C2/m), B2-type Al (Cu, Fe) (a=0.29 nm; cP2; $Pm\bar{3}m$) and $Al_{78}Cu_{48}Fe_{14}$ (a=b=c=1.231 nm; α=β=γ=90˚; cP140; $Pm\bar{3}$; PDF card no.: 01-073-7315) phase. The XRD pattern of the as-cast IQC followed by annealing at 800 ℃ is having all the major reflection corresponding to (222000), (311111), ($222\bar{0}$0), (400222), (422222), (244020) & ($466\bar{4}$0) planes of IQC. The (311111) reflection of IQC phase is understood as superlattice peak and hence it confirms the face-centred ordering of the IQC reinforcement used in the Al-IQC composite (nomenclature described in Chapter 2). Figure 4.2 (a) and (b) represents the morphology of gas-atomized AA 6082 Al alloy powder and as-cast+annealed IQC alloy powder crushed with vibratory ball mill, respectively. The as-received gas-atomized AA 6082 Al alloys are quasi-spherical in nature, and particle size varies in the range of 10 to 25 µm as evident from Figure 4.2 (a). On the other hand, the Al-Cu-Fe IQC as-cast and annealed particles are in the form of flakes, as seen in Figure 4.2 (b). The faceted and sharp edges of the IQC particles having a particle size in the range of 20 to 30 µm, make it a suitable reinforcement, capable for microstructural refinement.

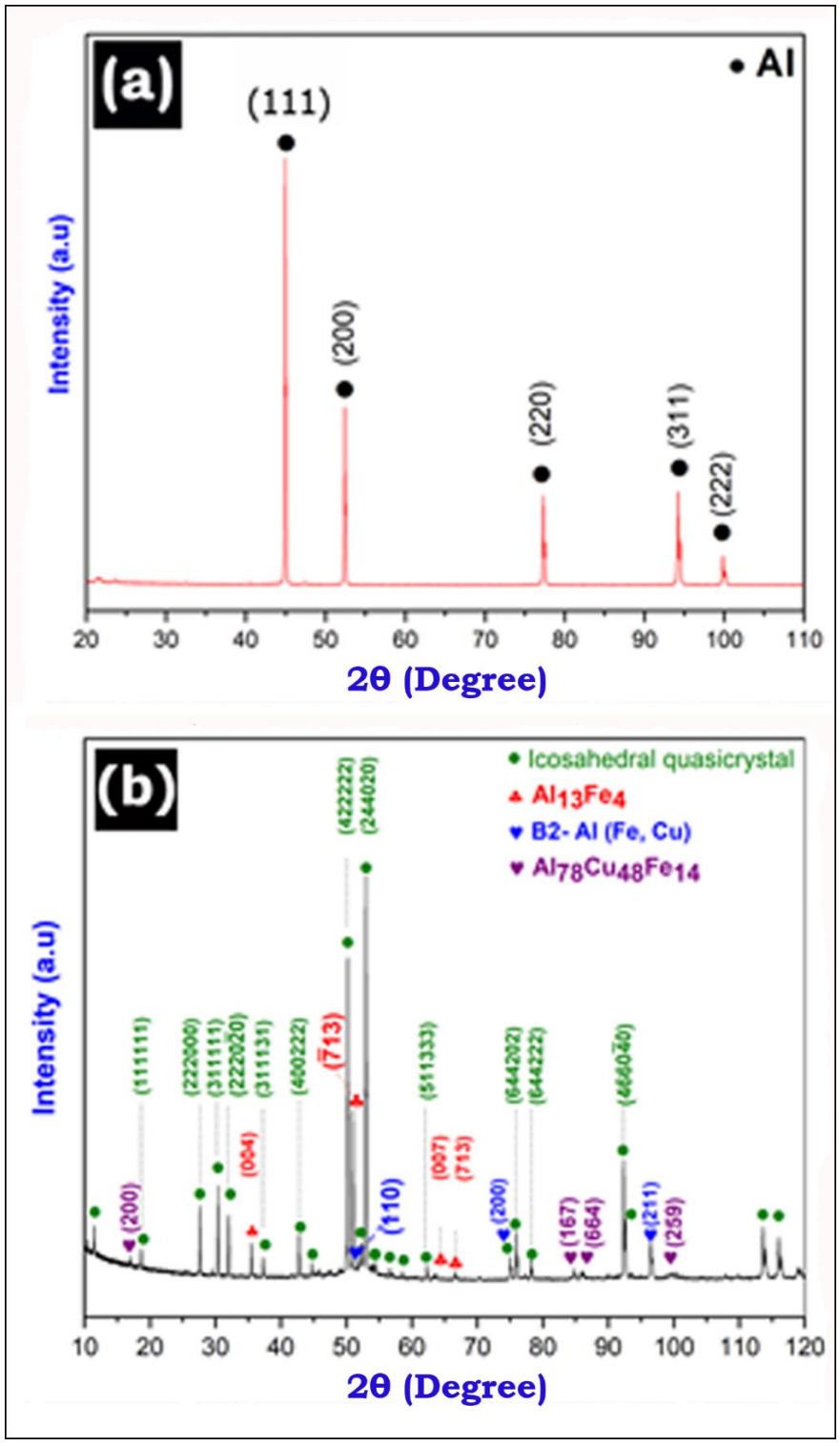

Figure 4. 1: Phase analysis of 6082 Al alloy (a) and as-cast and annealed Al-Cu-Fe IQC alloys (b).

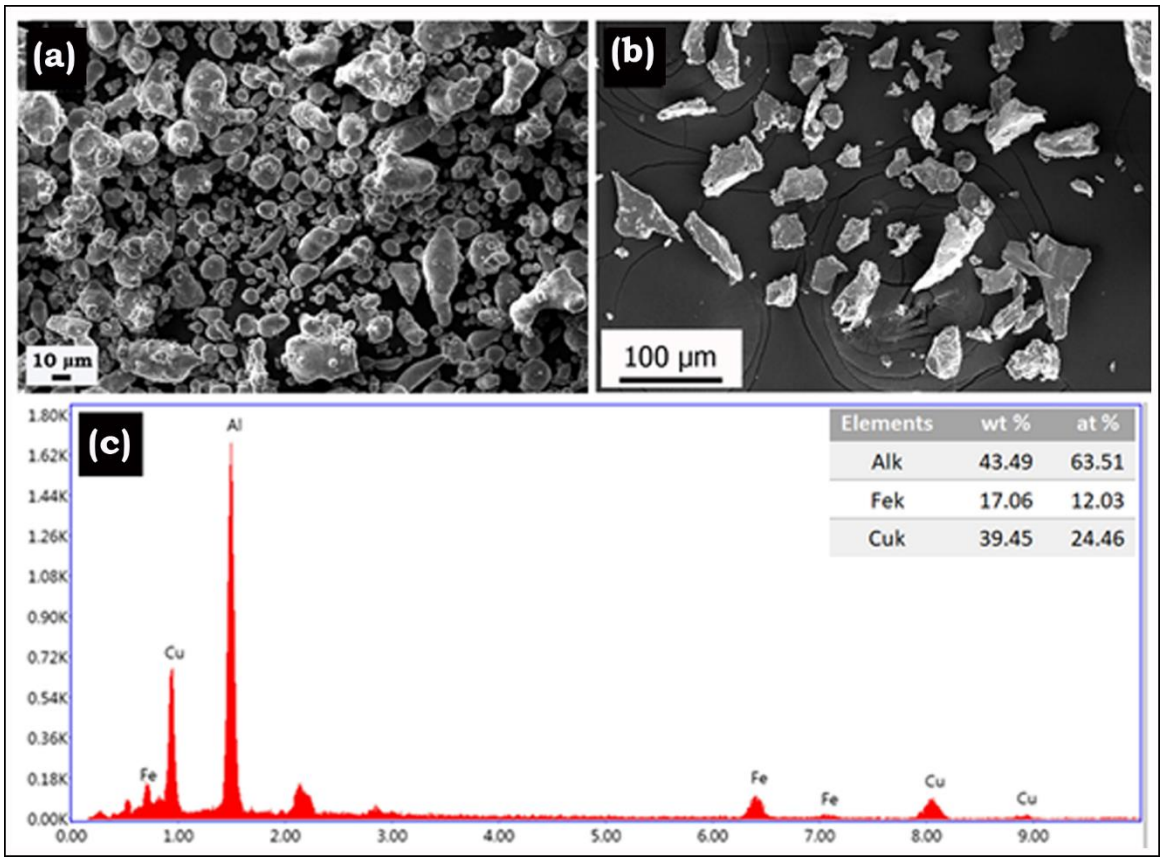

Figure 4. 2: SEM micrograph showing the morphology (a) of as received 6082 Al alloy and (b) as-cast & annealed Al-Cu-Fe IQC alloys; (c) EDS spectrum showing the chemical composition of as-cast and annealed Al-Cu-Fe IQC alloy.

The representative EDS spectrum and chemical composition of as-cast+annealed IQC alloy are shown in Figure 4.2 (c). From Figure 4.2 (c) it is evident that the chemical composition of as-cast+annealed IQC alloy powder is very close to the nominal composition of $Al_{62.5}Cu_{25}Fe_{12.5}$ (at%) without any presence of major peaks corresponding to that of the oxygen.

The Al alloy and Al–IQC composite having different volume fraction of reinforcement are MM as per the parameters described in the Chapter 2. Figure 4.3 represents the XRD pattern of AA 6082 Al alloy MM upto 50 h. During MM of Al alloy peak broadening was observed and no signature of Mg and Si was seen, confirming that these elements remain in the solid solution.

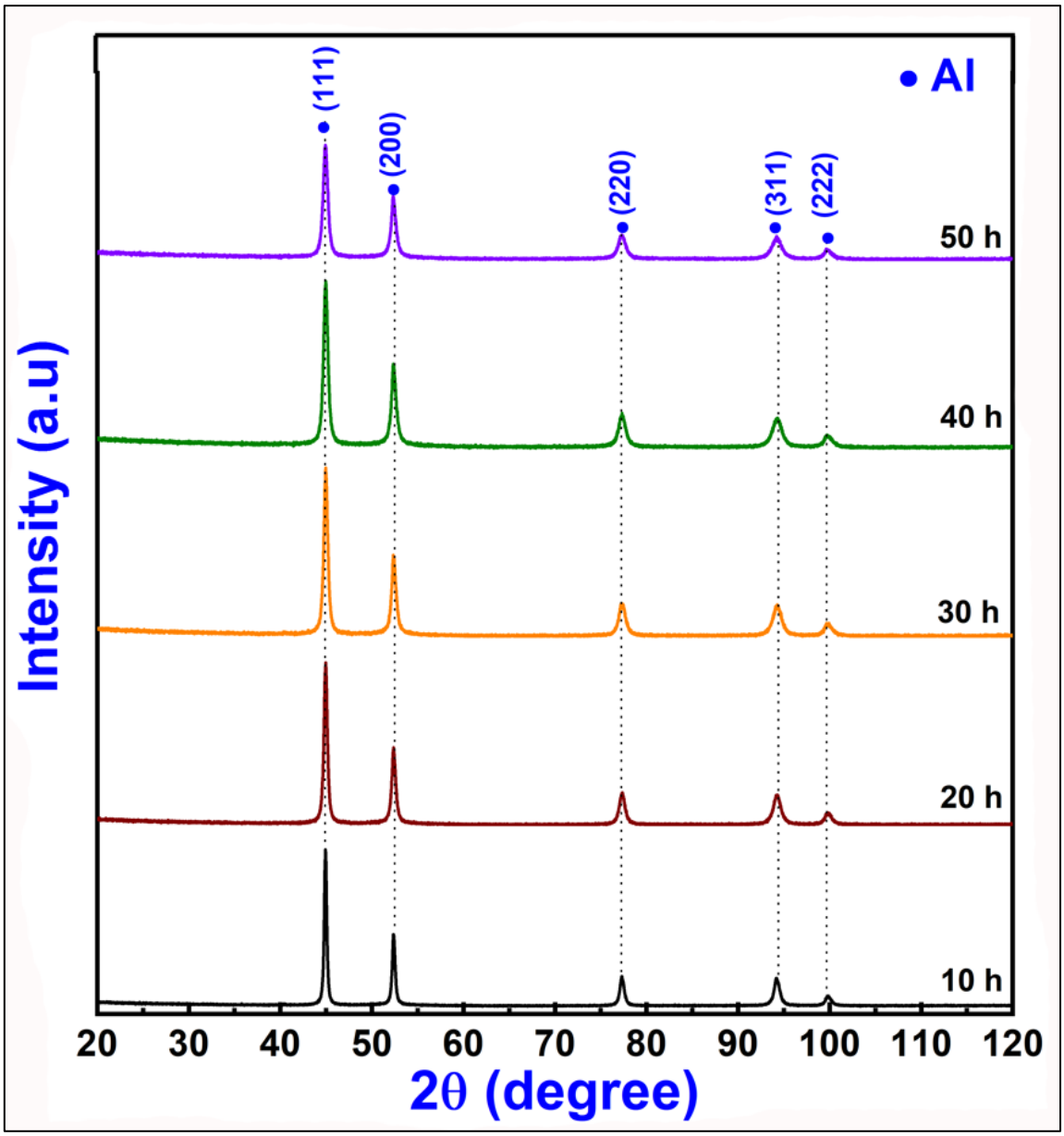

Figure 4. 3: X-ray diffraction pattern of AA 6082 Al alloy milled for various time duration.

The sequence of structural transformation during MM of Al-IQC nanocomposite powder can be discerned from the Figure 4.4 and 4.5 (a & b). During MM of Al–IQC nanocomposite powder having upto 30 vol% of IQC reinforcement, no signature of structural transformation of IQC phase was observed. However, this condition does not prevail for Al-40IQC nancomposite MM up to 50 h. During MM of Al-IQC

nanocomposite, significant amount of refinement was observed as illustrated from the crystallite size and lattice strain reported in Table 4.1.

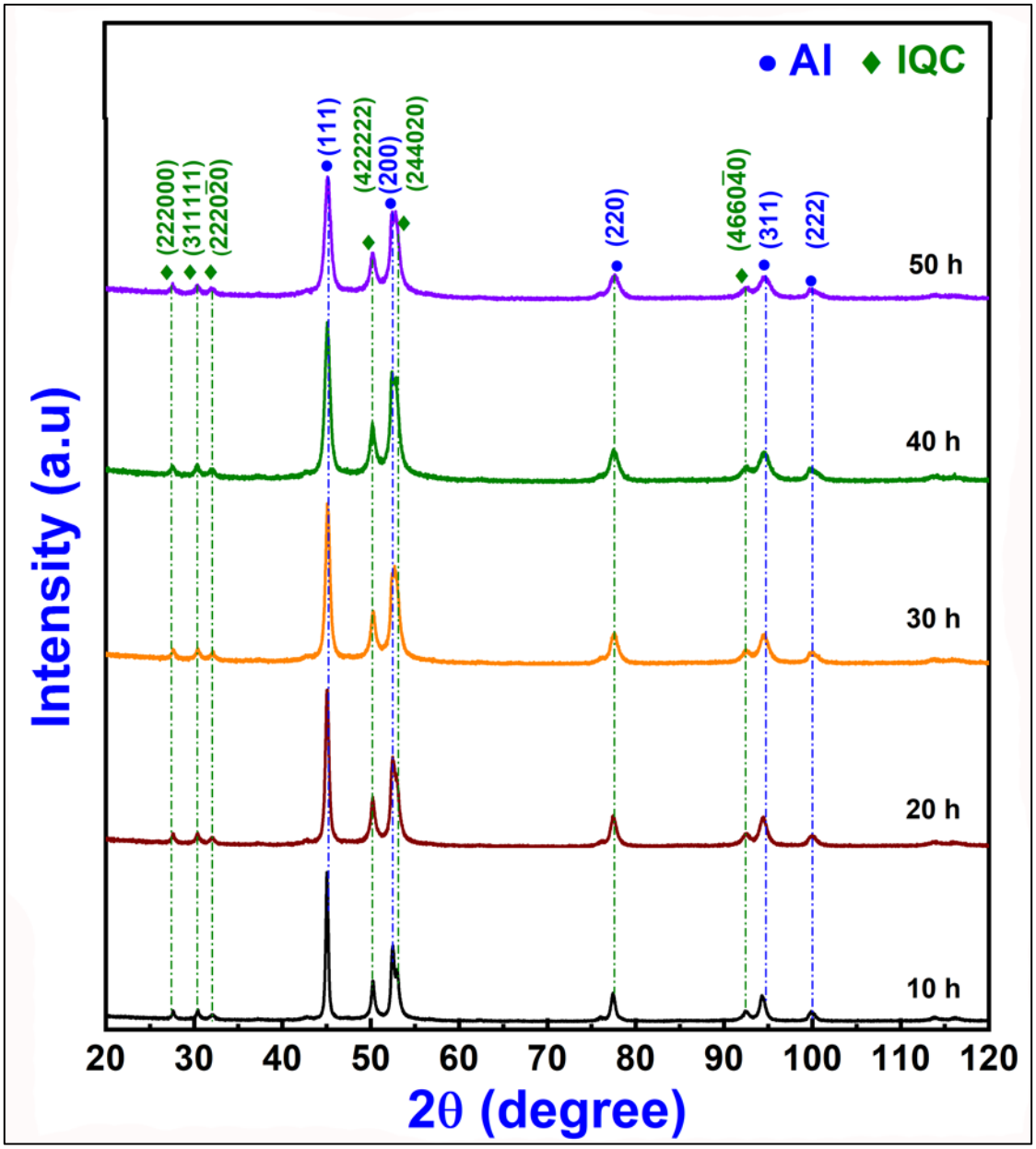

Figure 4. 4: X-ray diffraction pattern of Al-30IQC composite milled for various time duration.

Figure 4.5 represents the structural transformation during MM upto 50 h of 6082 Al matrix reinforced with 40 vol% of Al-Cu-Fe IQC. It is evident from Figure 4.5 (a) face-centred ordered IQC phase is able to retain its identity upto 50 h of MM.

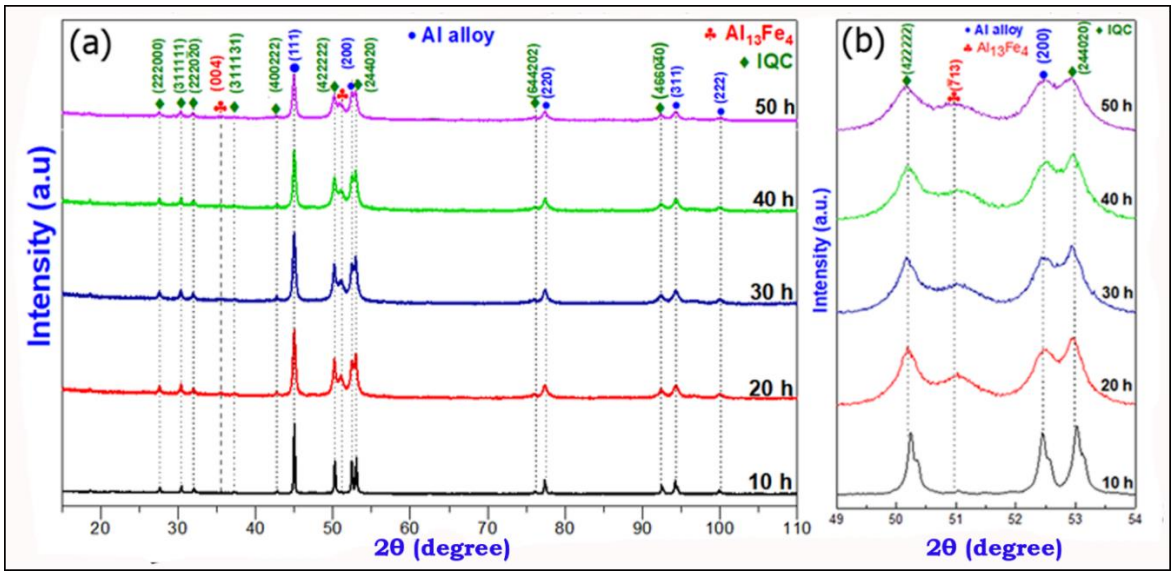

Figure 4. 5: Phase analysis of Al-40IQC NC powder MM upto 50h (a); Structural transformation of IQC phase and approximant phases in Al-40IQC NC powder MM upto 50 h (b).

Table 4. 1: Crystallite size and lattice strain during mechanical milling of Al – IQC nanocomposite powder.

Milling duration (h)	Al-0IQC		Al-10IQC		Al-20IQC		Al-30IQC		Al-40IQC	
	CS (nm)	LS (%)	CS (nm)	LS (%)	CS (nm)	LS (%)	CS (nm)	LS (%)	CS (nm)	LS (%)
10	205	0.055	162	0.084	145	0.086	131	0.087	121	0.089
20	61	0.177	46	0.287	42	0.307	40	0.330	37	0.347
30	49	0.204	30	0.335	25	0.359	22	0.377	18	0.402
40	42	0.218	25	0.385	22	0.392	20	0.402	16	0.432
50	37	0.233	24	0.395	20	0.437	18	0.461	16	0.488
Crystallite size (CS); Lattice strain (LS)										

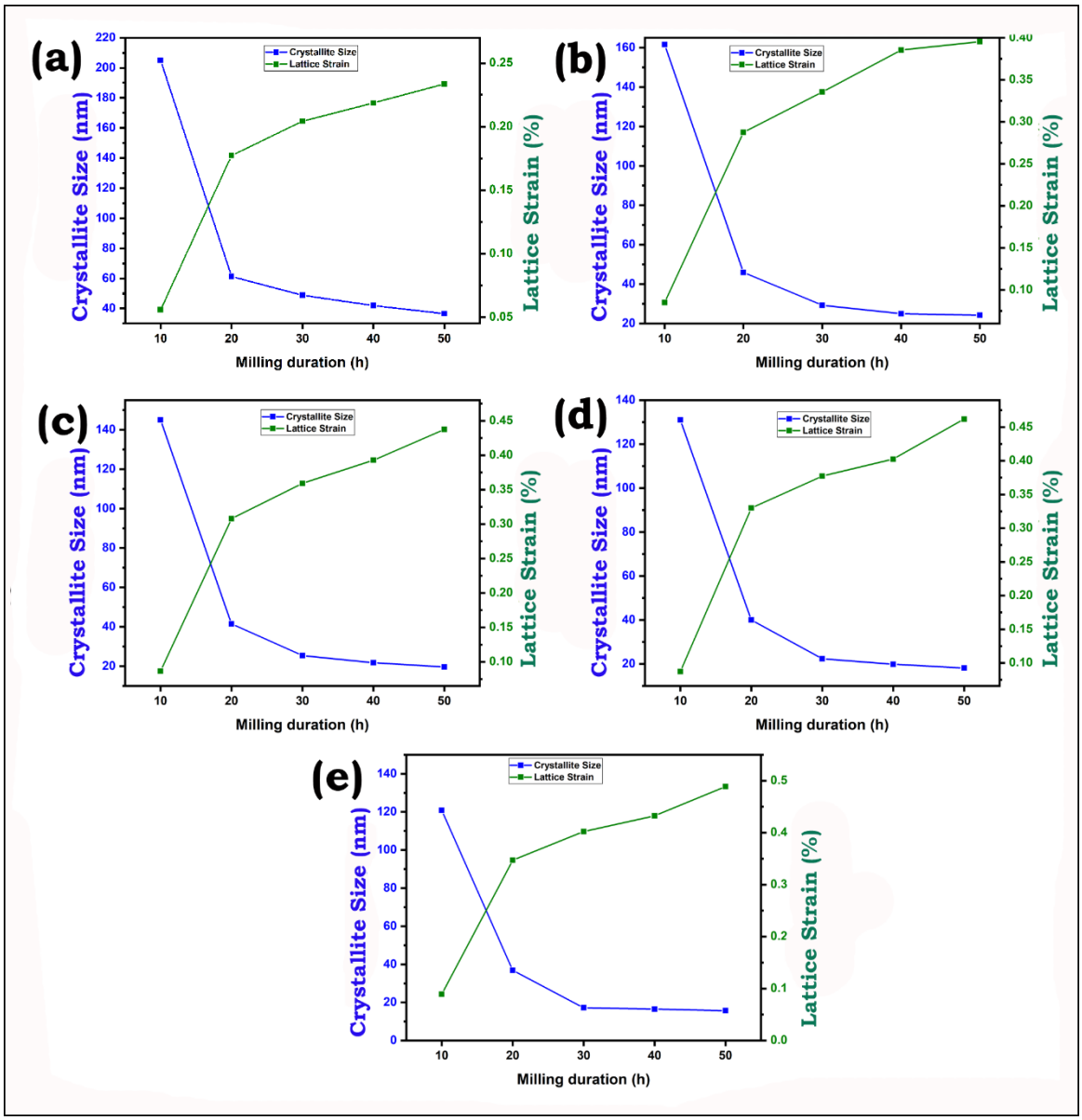

Figure 4. 6: Variation of crystallite size and lattice strain of (a) Al–0IQC, (b) Al–10IQC, (c) Al–20IQC, (d) Al–30IQC, (e) Al–40IQC nanocomposite powder after mechanical milling for various duration of time.

The minor fraction of crystalline phases seen in the as-cast+annealed IQC is not very significant after 10 h of MM in case of Al-40IQC AMCs. However, a minor fraction of the IQC phase transforms to $Al_{13}Fe_4$ phase subjected to 50 h of MM.

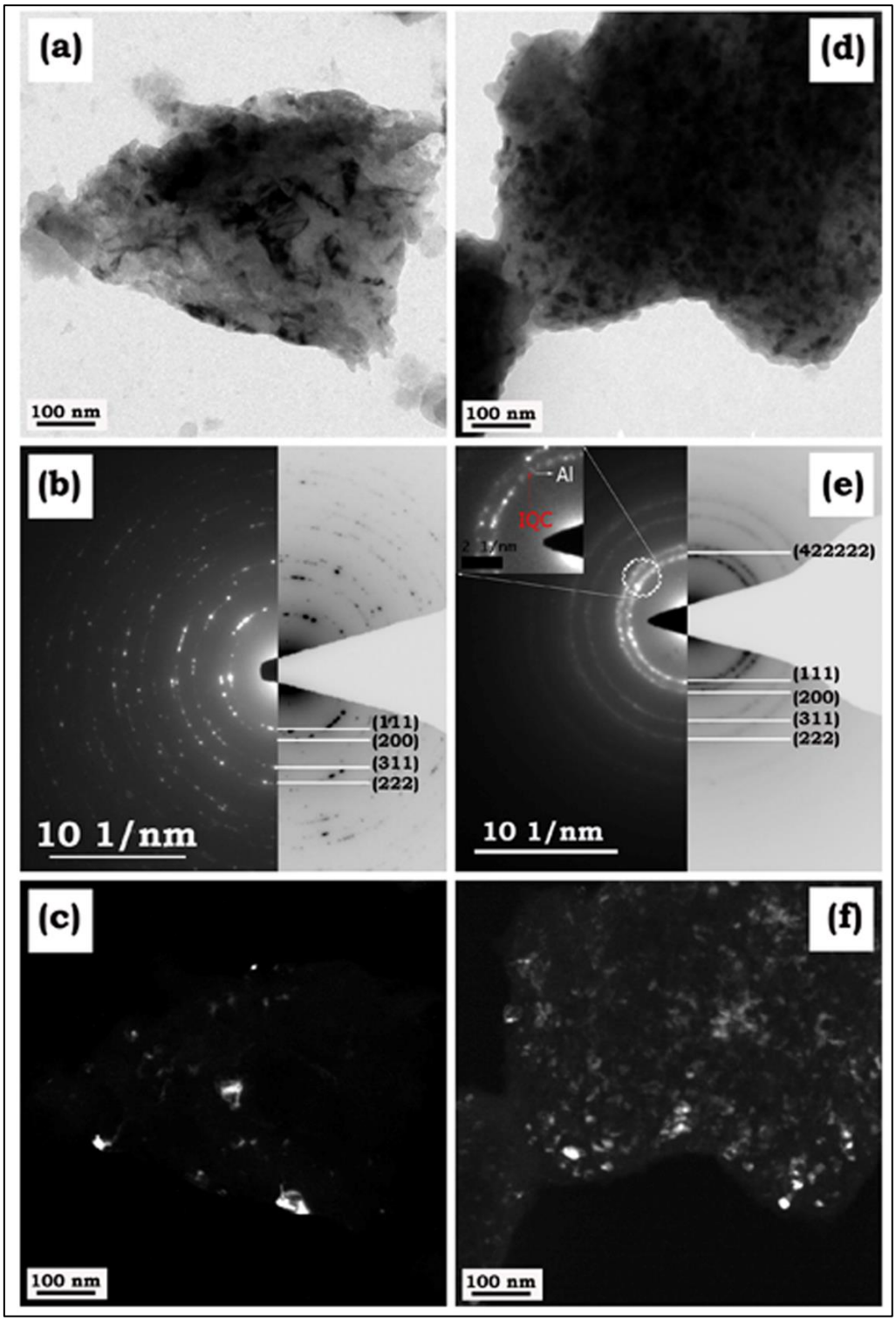

Figure 4. 7: Diffraction contrast images of Al-0IQC and Al-40IQC NC powder MM upto 50 h. Bright-field image of (a) Al-0IQC and (d) Al-40IQC NC powder; the SAD pattern of (b) Al-0IQC and (e) Al-40IQC NC powder; Darkfield image of (c) Al-0IQC and (f) Al-40IQC NC powder.

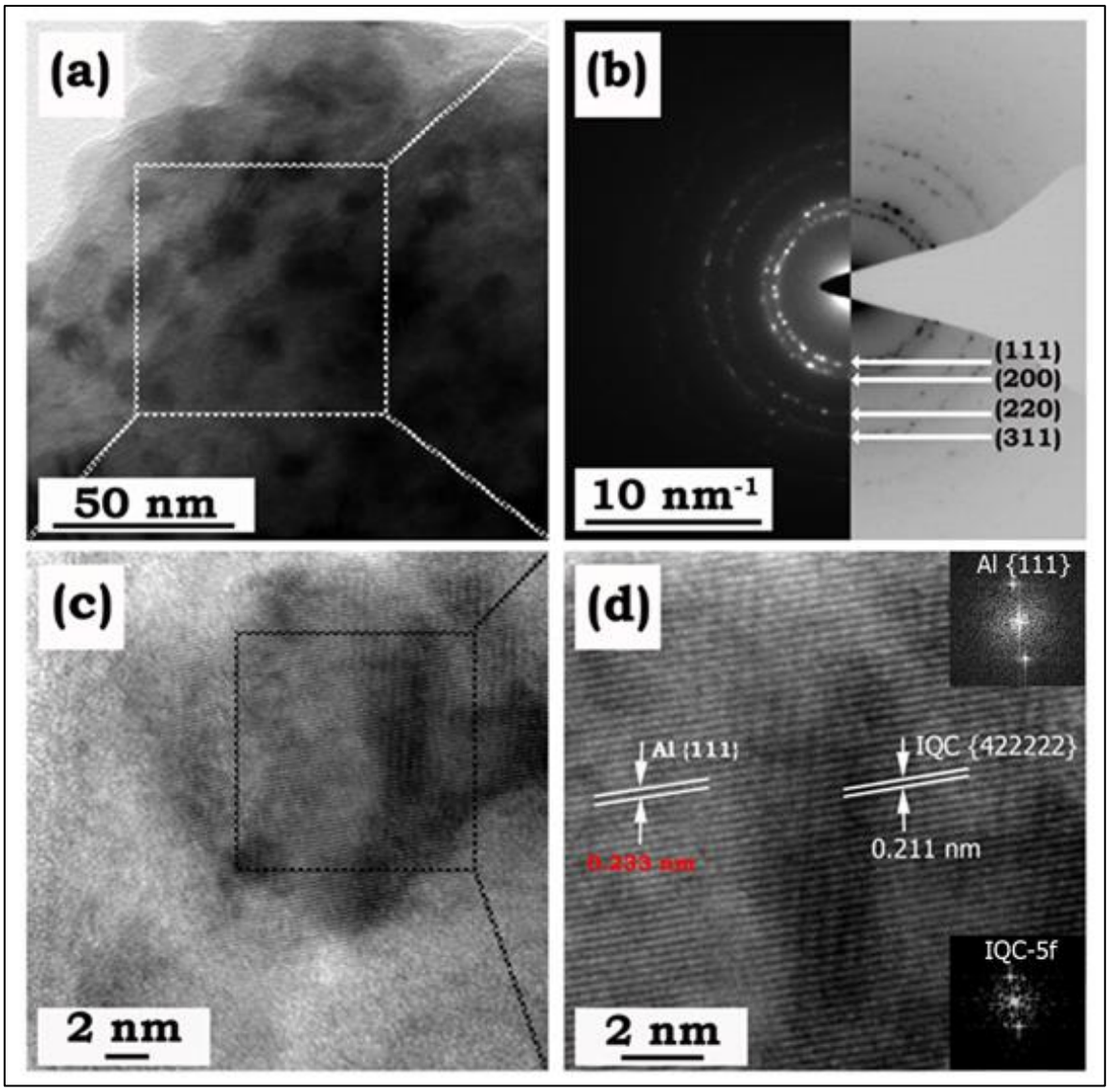

Figure 4. 8: Representative TEM image (a), corresponding SAD pattern (b), HRTEM image (c) and (d) magnified HRTEM image of Al-40IQC NC powder MM upto 50 h.

.

The preferential structural transformation of IQC phase to $Al_{13}Fe_4$ phase corresponding to $(\bar{7}13)$ reflection was evident from Figure 4.7 (b). It is also evident that the phase fraction of $(\bar{7}13)$ reflection of $Al_{13}Fe_4$ phase increases as a function of MM duration in Al-40IQC AMCs powder. During MM, the Al-40IQC nanocomposite powder is subjected to repetitive collision, fracture and cold welding. The aperiodic intermetallics also enhances the microstructural refinement and increases the lattice strain of the Al matrix

in Al-IQC nanocomposite powder. The crystallite size and lattice strain variation are evident from Figure 4.6 and Table 4.1.

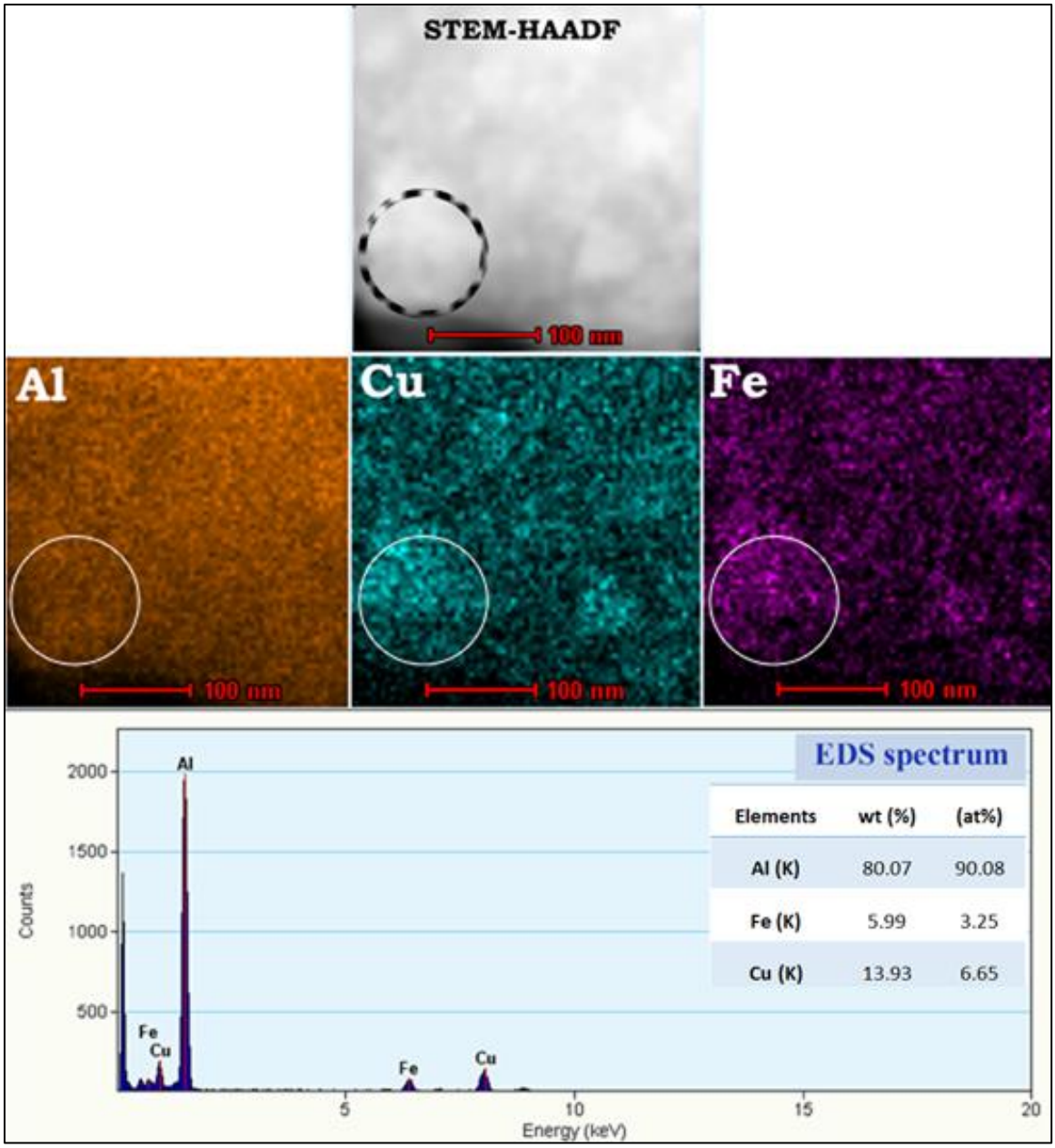

Figure 4. 9: HAADF-STEM-EDS elemental map and corresponding EDS spectrum showing the distribution of Al, Cu and Fe in Al-40IQC NC powder MM upto 50 h.

It is evident that the hard, aperiodic intermetallics is capable enough for grain refinement of Al matrix upto ~ 16 nm with high lattice strain of ~0.488% for Al-40IQC nancomposite powder. However, it can be discerned from the Figure 4.6 and Table 4.1 that

increase in volume fraction of IQC from 30 to 40 in Al alloy does not have siginificant rise in the level of crystallite size refinement and any fruther increase in the volume fraction might have lead to the saturation in the crystallite size refienement.

4.1.2 TEM investigation of Al-IQC nanocomposite powder

The diffraction contrast images of Al alloy and Al-40IQC NC powder MM upto 50 h is shown in Figure 4.7 (a-c) and Figure 4.7 (d-f) respectively. The bright-field (BF) image and corresponding selected area diffraction (SAD) pattern along with the dark field (DF) image are shown in Figure 4.7 (a), 4.7 (b) and 4.7 (c) respectively for Al alloys. Similarly, bright-field (BF) image and corresponding selected area diffraction (SAD) pattern along with the dark field (DF) image are shown in Figure 4.7 (d), 4.7 (e) and 4.7 (f) respectively for Al-40IQC nanocomposite powder MM upto 50 h. A few dark regions are observed in the BF image of Al alloys MM upto 50 h. It has been long established that dark patches of mottled contrast in diffraction contrast images are mainly due to the strain accumulation. A similar contrast is observed in the current investigation. Moreover, the processing history of the material makes this case even more relevant as in mechanical milling strain accumulation does happen.

Figure 4.7 (b) shows the representative polycrystalline SAD pattern for Al alloys, ascertaining the random orientation of grains in the Al alloys subjected to MM for a prolonged duration. Figure 4.7 (c) represents the DF image of Al alloy corresponding to (111) reflection of α-Al. It is evident from the DF image that severe plastic deformation during MM has led to grain size refinement of α-Al alloy less than 50 nm.

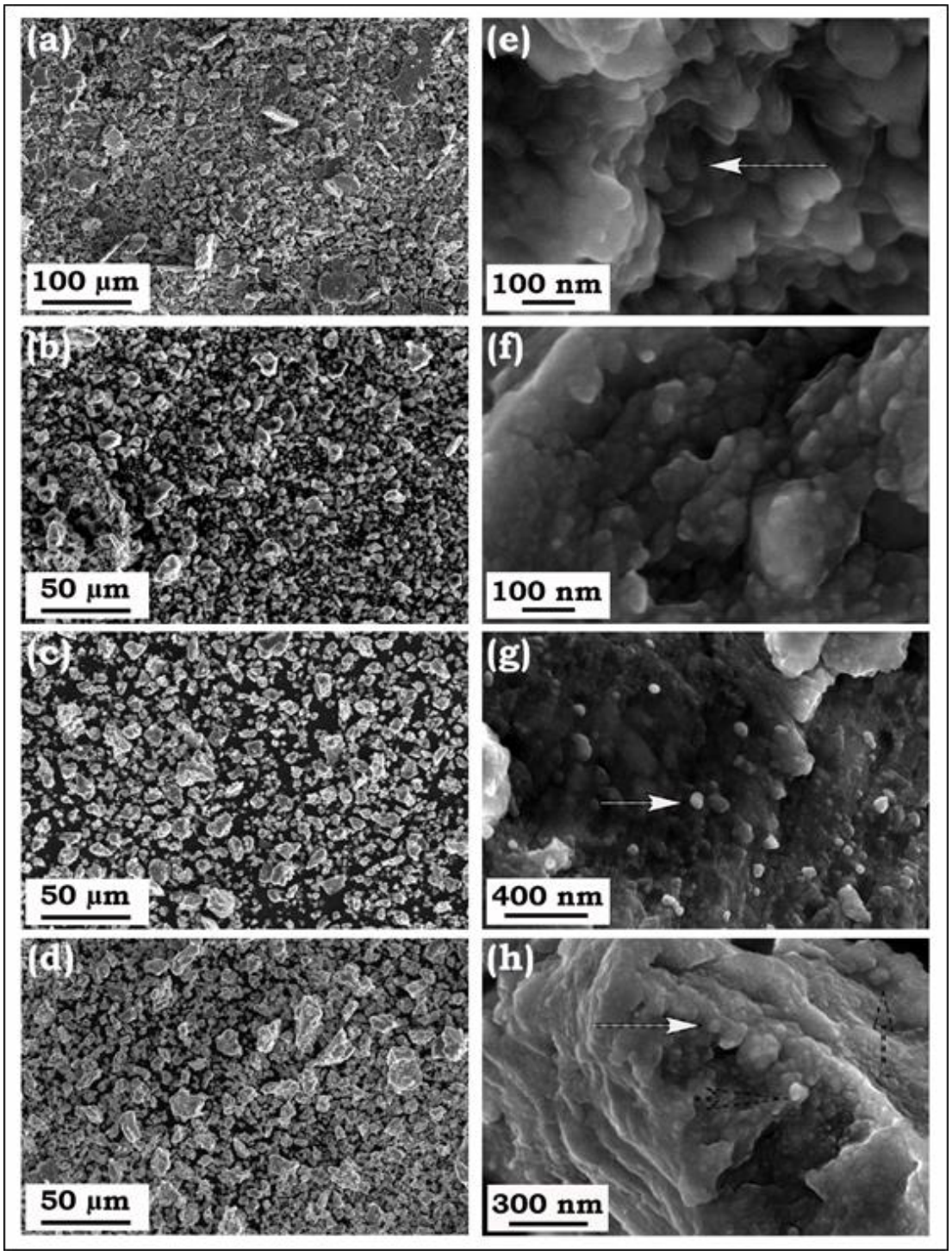

Figure 4. 10: SEM micrograph showing the morphology and nanostructured grains in (a, e) Al-0IQC, (b, f) Al-10IQC, (c, g) Al-20IQC, (d, h) Al-30IQC nanocomposite powder MM for 50 h.

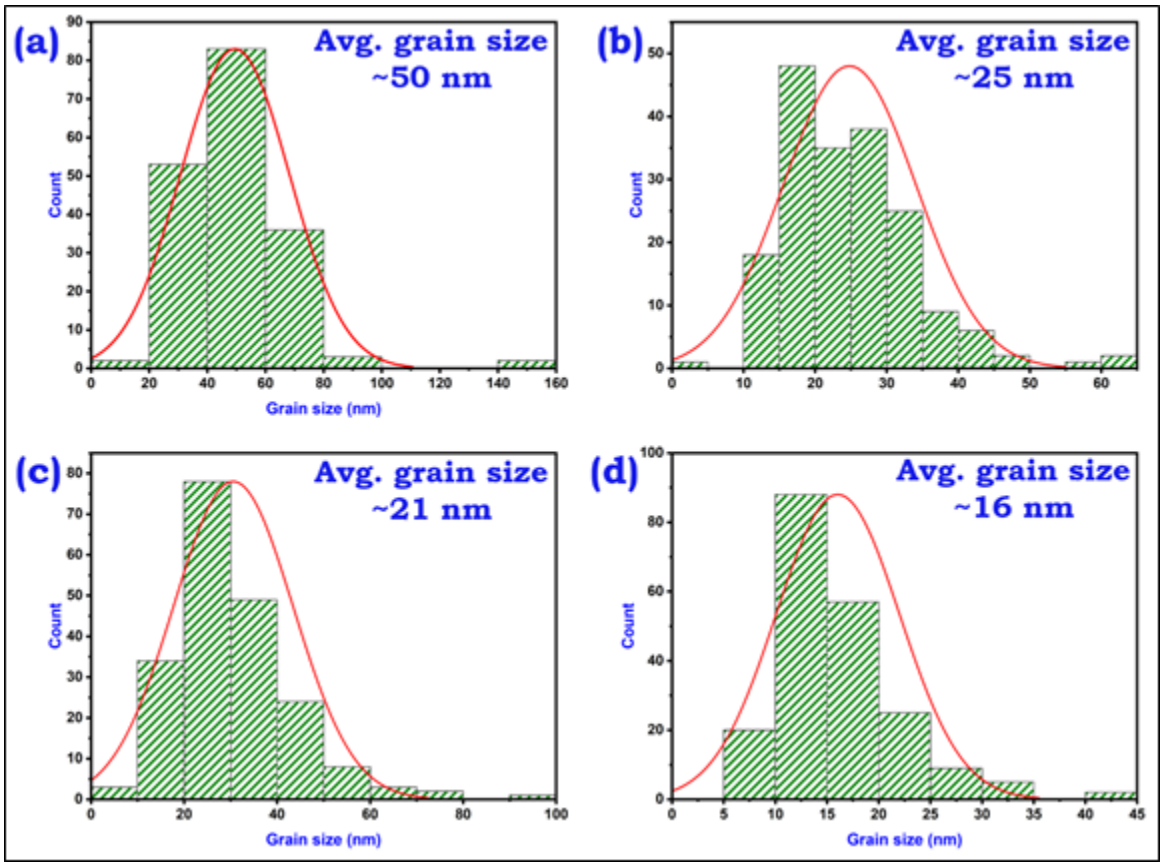

Figure 4. 11: Grain size distribution of (a) Al–0IQC, (b) Al–10IQC, (c) Al–20IQC, (d) Al–30IQC nanocomposite powder mechanically milled for 50 h.

Similarly, in Al-40IQC, many dark patches corresponding to strain accumulation and IQC reinforcement are seen (Figure 4.7 (d)). The increase in the fraction of dark region in Al-40IQC in comparison to Al alloy is due to enhanced microstructural refinement during severe plastic deformation of Al matrix in the presence of hard aperiodic reinforcement of Al-Cu-Fe IQC particles. Figure 4.7 (e) shows representative polycrystalline SAD pattern having major reflection corresponding to α-Al. The random orientation and enhanced microstructural refinement during MM of Al-40IQC are evident from the thick polycrystalline diffraction rings of α-Al as evident from Figure 4.7 (e). The careful observation of diffraction rings shows the presence of (422222) nano-quasicrystalline plane of Al-Cu-Fe IQC phase having interplanar spacing (d ~ 0.211 nm)

very close to that of the (111) reflection of α-Al (d ~ 0.233 nm). The co-existence of reflection corresponding to the Al matrix and IQC reinforcement was also evident from the powder XRD pattern of Figure 4.3. The DF image shows the formation of a nanostructured grain of matrix (≤ 20 nm) during HEBM upto 50 h for Al-40IQC NC powder. The size of the nano-structured grains formed after 50 h of MM, observed through TEM may be substantiated by the crystallite size of Al matrix as evident from the powder XRD pattern of Al-40IQC NC powder as seen in Table 4.1.

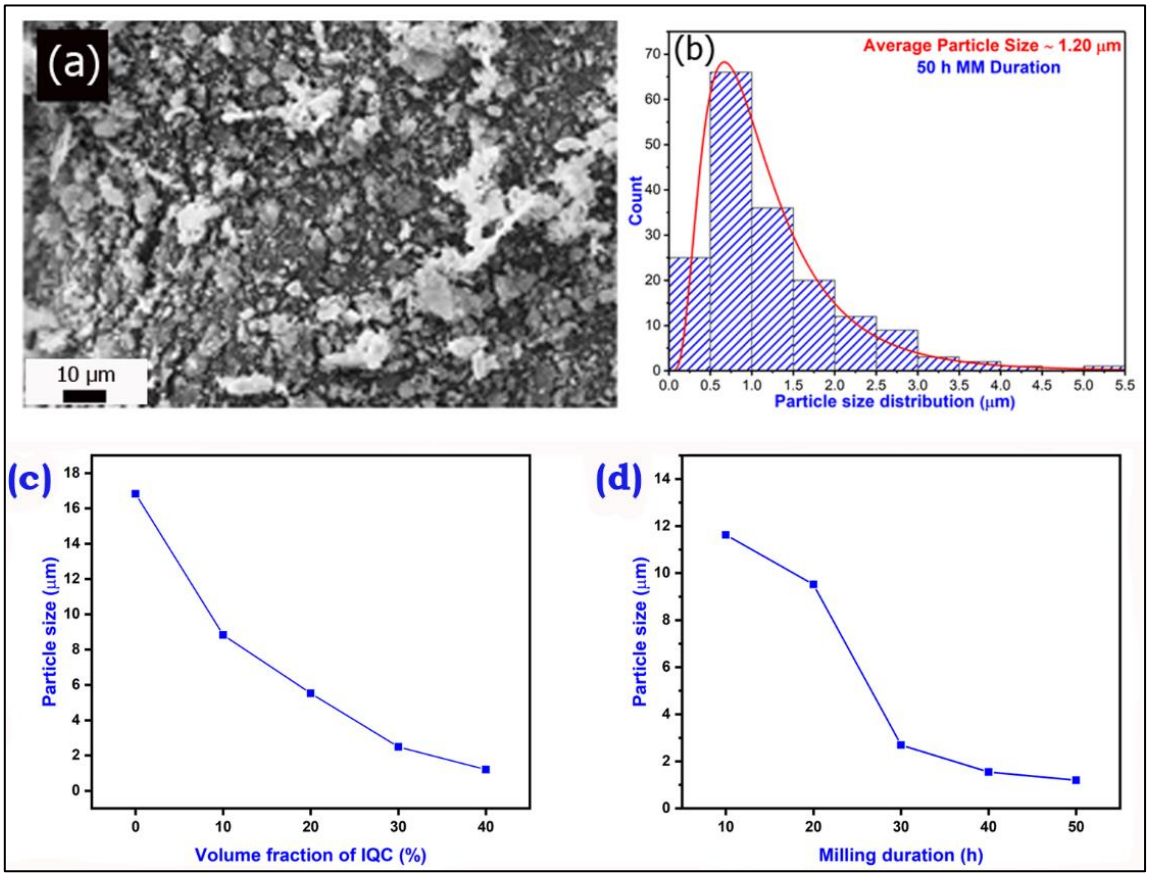

Figure 4. 12: (a and b) Morphology and particle size distribution of Al-40IQC MM for 50 h respectively; (c) variation of particle size w.r.t volume fraction of reinforcement; (d) variation of particle size w.r.t milling duration in Al-40IQC NC powder.

The grain refinement observed through TEM is almost comparable that observed through XRD. The interaction volume for XRD and TEM are different. In the case of XRD,

a large area with higher thickness contributes compared to that of the localized narrow region for TEM. The grain size observed in the case of TEM corresponds to the particular particle which had been investigated through diffraction contrast images in the thin region at the edges of the powder particles. Figure 4.8 shows the phase contrast image of Al-40IQC NC powder MM upto 50 h.

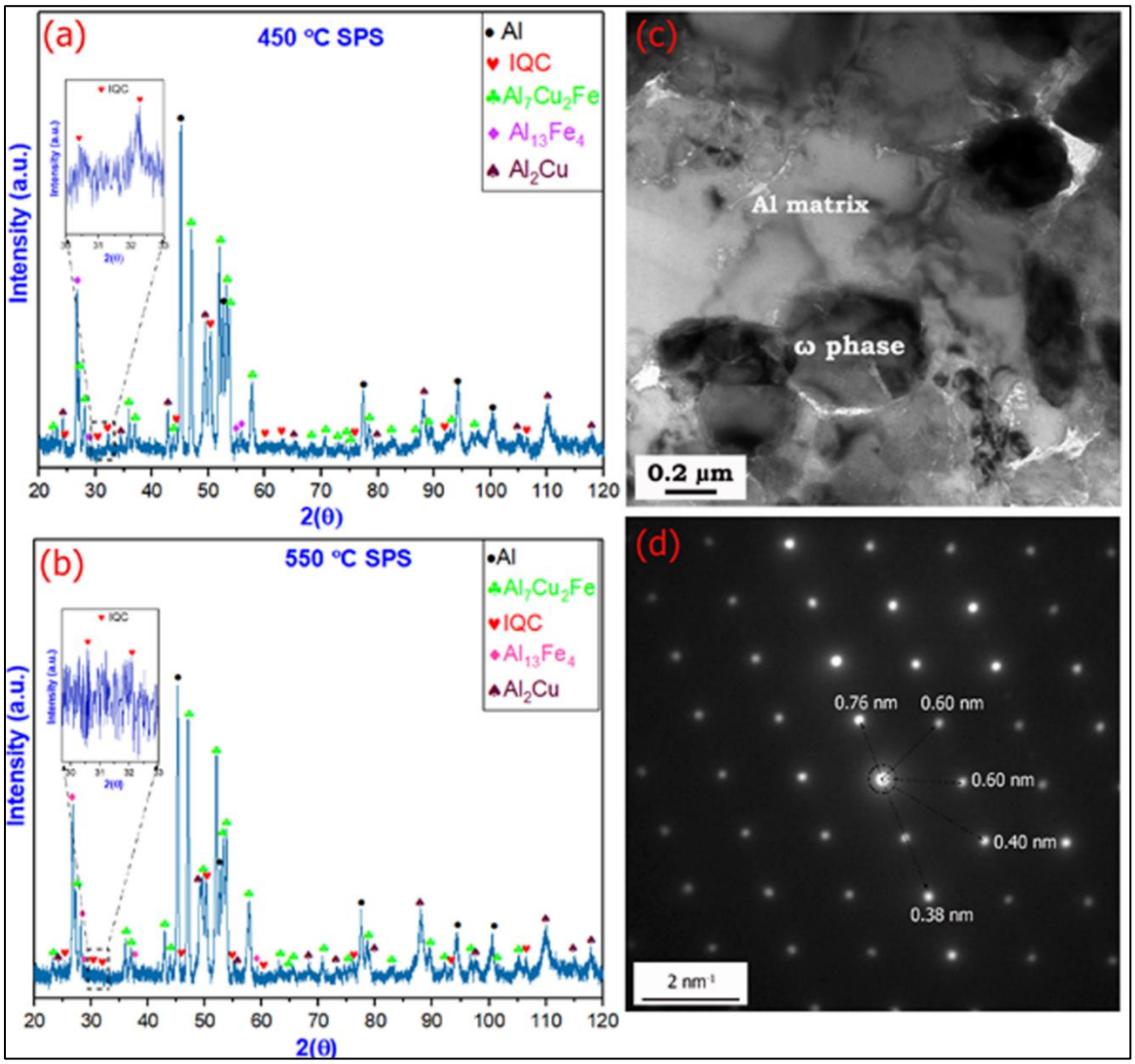

Figure 4. 13: Phase analysis of Al-40IQC NC powder SPSed at (a) 450 °C and (b) 550 °C; Diffraction contrast image showing (c) Bright field and (d) SAD pattern of Al-40IQC composite SPSed at 550 °C.

Figure 4.8 (a) shows the representative TEM image of NC powder showing the region of phase-contrast imaging having reinforcement and dark patches due to strain

accumulation. The SAD pattern is shown in Figure 4.8 (b) having all major reflection corresponding to FCC-Al. Figure 4.8 (c & d) represents the HRTEM image of Al-40IQC. The lattice fringes having interplanar spacing (d~0.233 nm) corresponding to (111) reflection of FCC-Al is quite evident. The interfacial coherency of the (111) plane of Al matrix with (422222) plane of IQC reinforcement may be seen in Figure 4.8 (d).

The lattice fringe having interplanar spacing (d~0.211 nm) corresponding to (422222) reflection of IQC phase is also evident from Figure 4.8 (d). This result is substantiated by powder XRD pattern showing the presence of all major reflection of FCC-Al and IQC phase (Figure 4.5). Further, Figure 4.9 represents the HAADF-STEM-EDS elemental map and its corresponding EDS spectrum of Al-40IQC NC powder. The elemental map shows uniform distribution of Al, and patches corresponding to Cu and Fe may also be seen in the STEM-EDS map. The STEM-EDS map establishes the homogenous distribution of the IQC phase in the Al matrix, which is well embedded in the matrix with good interfacial integrity. The region rich in Al, Cu and Fe, corresponding to IQC are marked with circles in Figure 4.9.

4.2 Morphology of Al-IQC nanocomposite powder

The morphology and grain size distribution of Al – IQC NC powder having upto 30 vol% of reinforcement are shown in the Figure 4.10. The Figure 4.10 (a), (b), (c) and (d) represent the shape, size and morphology of the powder Al-0IQC, 10IQC, 20IQC and 30IQC NC powder MM for 50 h. The nano-structured grains formed during MM of Al-0IQC, 10IQC, 20IQC and 30IQC NC powder was discerned from the Figure 4.10 (e), (f), (g) and (h) respectively. The grain size distribution of Al-IQC nanocomposite powder is shown in the Figure 4.11. It can be observed from the Figure 4.11 that the level of grain refinement is significant for Al-30IQC and an average grain size of ~16 nm was observed.

Further, it can be discerned that for the Al-20IQC and Al-30IQC shown in the Figure 4.10 (g) and (h), the IQC particles are well embedded in the Al matrix and have good interfacial bonding.

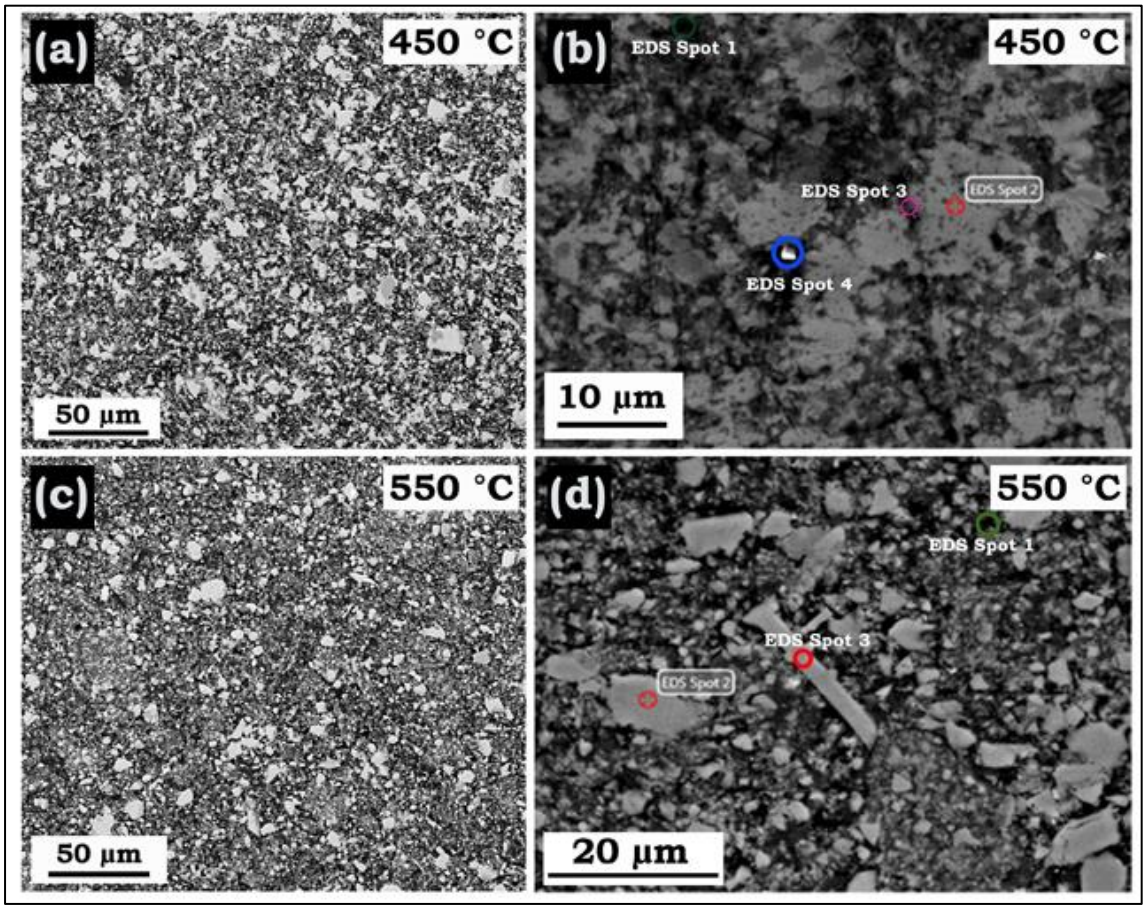

Figure 4. 14: Back-scattered SEM micrograph showing the distribution of Al matrix and reinforcement particles at different magnification for Al-40IQC NC powder SPSed at 450 ℃ (a & b) and 550 ℃ (c & d).

The morphology and particle size distribution of AA 6082 Al matrix reinforced with 40 vol% of Al-Cu-Fe IQC particles MM upto 50 h is evident from Figure 4.12 (a) and (b). In the case of the Al-40IQC. The variation of the particle size of the Al matrix in Al-IQC w.r.t the volume fraction of IQC reinforcement is represented in the Figure 4.12 (c). Increasing the volume fraction of IQC, the level of refinement of the particles also

increases. The particle size refinement of Al matrix in Al-40IQC was maximum and observed to be ~1.2 μm.

Table 4. 2: Elemental composition of phases in Al-40IQC composite SPSed at 450 ℃ (723 K) and 550 ℃ (823 K).

SPS Temperature	Region	Al		Fe		Cu		Mg		Si	
		wt %	at %	wt %	at %	wt %	at %	wt %	at %	wt %	at %
450 ℃	**Spot-1**	84.20	91.50	5.20	2.70	9.30	4.30	0.70	0.90	0.60	0.60
	Spot-2	54.40	72.90	15.30	9.90	30.20	17.20	-	-	-	-
	Spot-3	65.90	80.70	10.70	6.30	22.30	11.60	0.70	0.90	0.40	0.50
	Spot-4	27.40	32.00	3.50	2.00	19.20	9.50	3.00	3.50	46.90	52.60
550 ℃	**Spot-1**	79.70	89.00	6.50	3.50	12.60	6.00	0.90	1.10	0.40	0.40
	Spot-2	53.50	71.50	16.40	10.60	29.10	16.50	0.60	0.90	0.40	0.50
	Spot-3	54.40	72.00	18.30	11.70	26.30	14.80	0.60	0.80	0.50	0.70

Further, systematic study were conducted to investigate the effect of MM in the microstructural refinement of Al-40IQC NC powder as shown in the Figure 4.12 (d). The microstructural refinement of Al matrix in Al-40IQC NC powder is considerable upto 20 h of MM, and with the fragmentation of IQC particles, the intensity of microstructural refinement of Al matrix is still appreciable upto 30 h of MM. However, after 30 h of MM, steady-state of refinement is observed for MM of Al-40IQC in between 30 h and 50 h. In Figure 4.6 and 4.12 (d), it may be clearly seen that the crystallite size refinement and particle size variation achieve steady-state after 30 h of MM.

4.3 Spark plasma sintering of Al-IQC composite

The Al-IQC composite was consolidated using spark plasma sintering (SPS). For SPS of Al-IQC, two types of sets of processing parameters were chosen to optimize the processing condition and details of the same are described in the Chapter 2. In one methodology, the Al-40IQC was SPSed at 450 ℃ (723 K), and 550 ℃ (823 K) at low pressure of 50 MPa. In another, methodology Al-0IQC, 10IQC, 20IQC, and 30 IQC were sintered at 300 ℃ (573 K) with a pressure of 500 MPa.

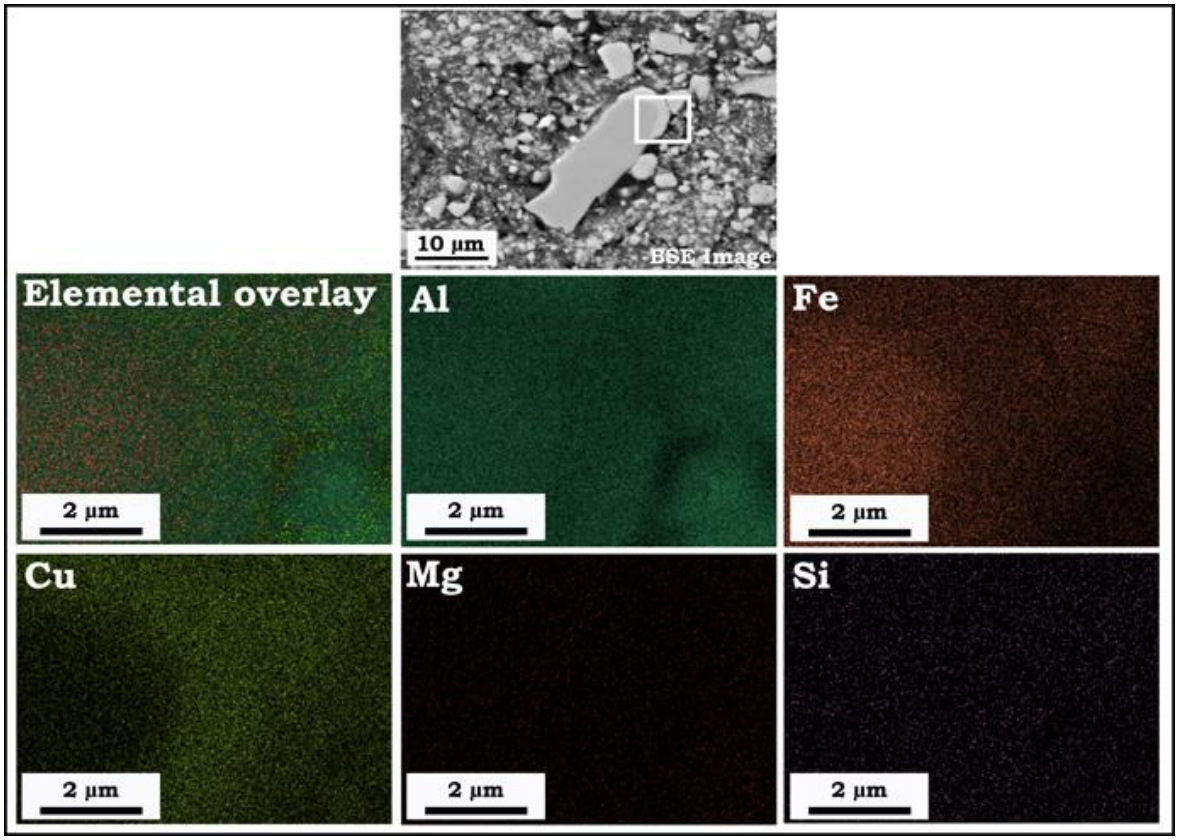

Figure 4. 15: SEM-EDS elemental map showing the distribution of Al, Fe, Cu, Mg and Si in Al-40IQC composite SPSed at 450 ℃ at the interface of matrix and reinforcement.

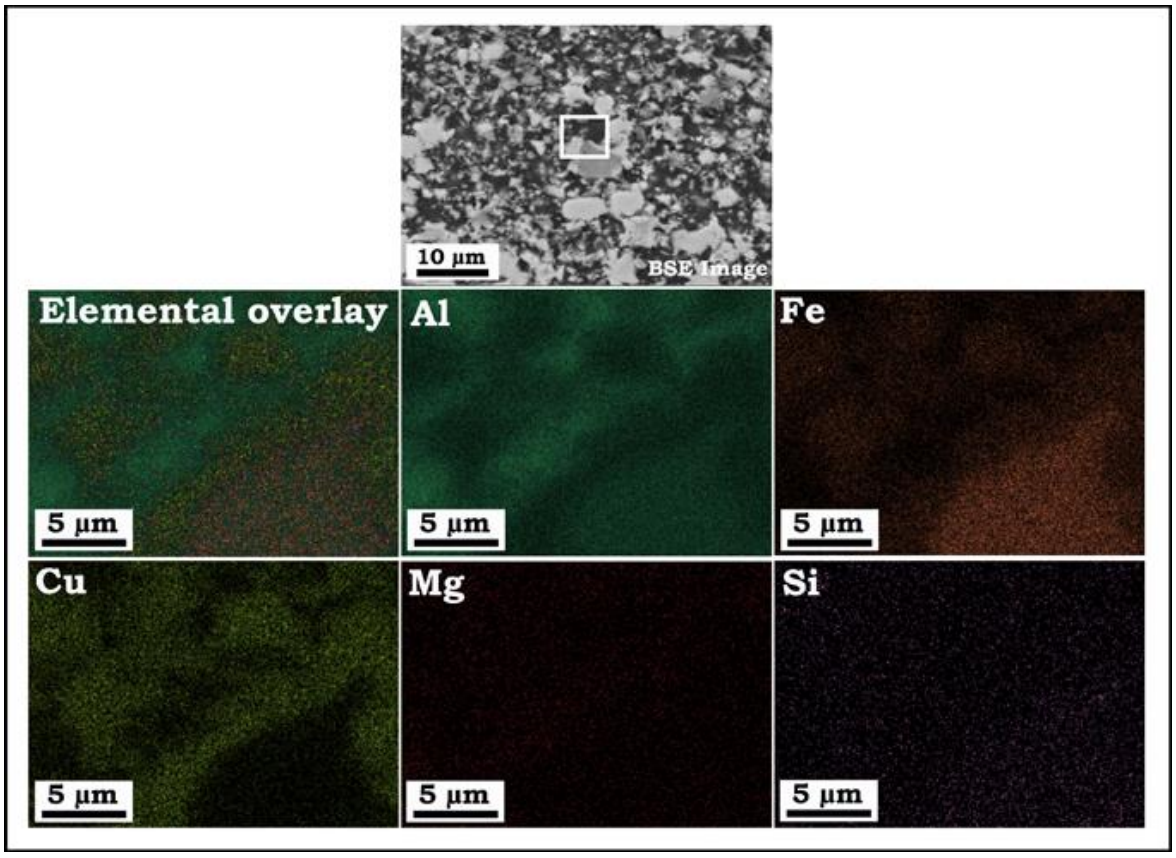

Figure 4. 16: SEM-EDS elemental map showing the distribution of Al, Fe, Cu, Mg and Si in Al-40IQC composite SPSed at 550 ℃ at the interface of matrix and reinforcement.

For studying the interfacial reaction and phase evolution during consolidation, SPS at 450 ℃ (723 K), and 550 ℃ (823 K) was employed. The phase analysis of Al-40IQC NC powder SPSed is done through XRD analysis and TEM investigation. Figure 4.13 (a) and (b) represents the powder XRD pattern for Al-40IQC composite SPSed at 450 ℃ (723 K) and 550 ℃ (823 K) respectively. It is evident from Figure 4.13 (a & b) that during sintering of Al-40IQC through SPS crystalline phases of IQC are formed. The SPS led to formation of θ-Al_2Cu (PDF card no.: 65-2695; a=b=0.6066 nm, c=0.4874 nm, α=β= γ=90˚; tI12; I4/mcm), λ-$Al_{13}Fe_4$ (PDF card no.: 65-1257; (a=1.549 nm, b=0.808 nm, c=1.248 nm, α=β=90˚, γ=107.720˚; mC102; C2/m) and ω-Al_7Cu_2Fe (PDF card no.: 25-1121;

a=b=0.6336 nm, c=1.487 nm, α=β= γ=90˚; tP40; P4/mnc) as evident from Figure 4.13 (a & b).

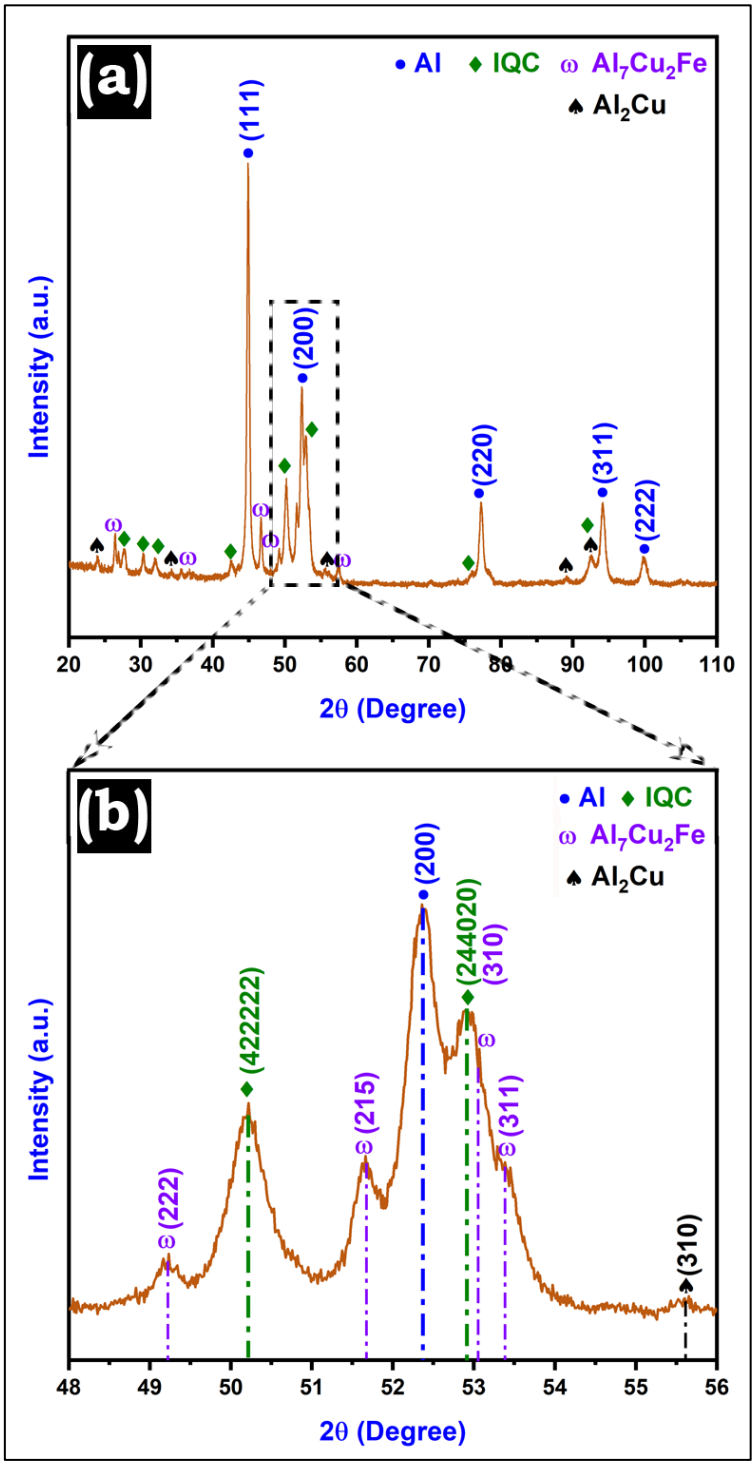

Figure 4. 17: Phase analysis of Al-30IQC SPSed at 300 ℃ (573 K) with a pressure of 500 MPa; (b) enlarged view showing the co-existence of Al, IQC and crystalline phases.

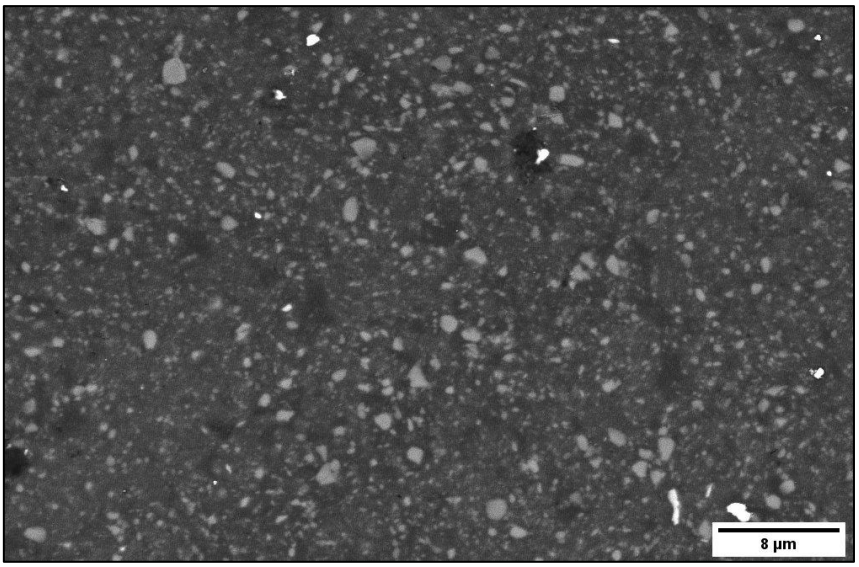

Figure 4. 18: BSE-SEM micrograph of Al-30IQC SPSed at 300 ℃ (573 K) with a pressure of 500 MPa.

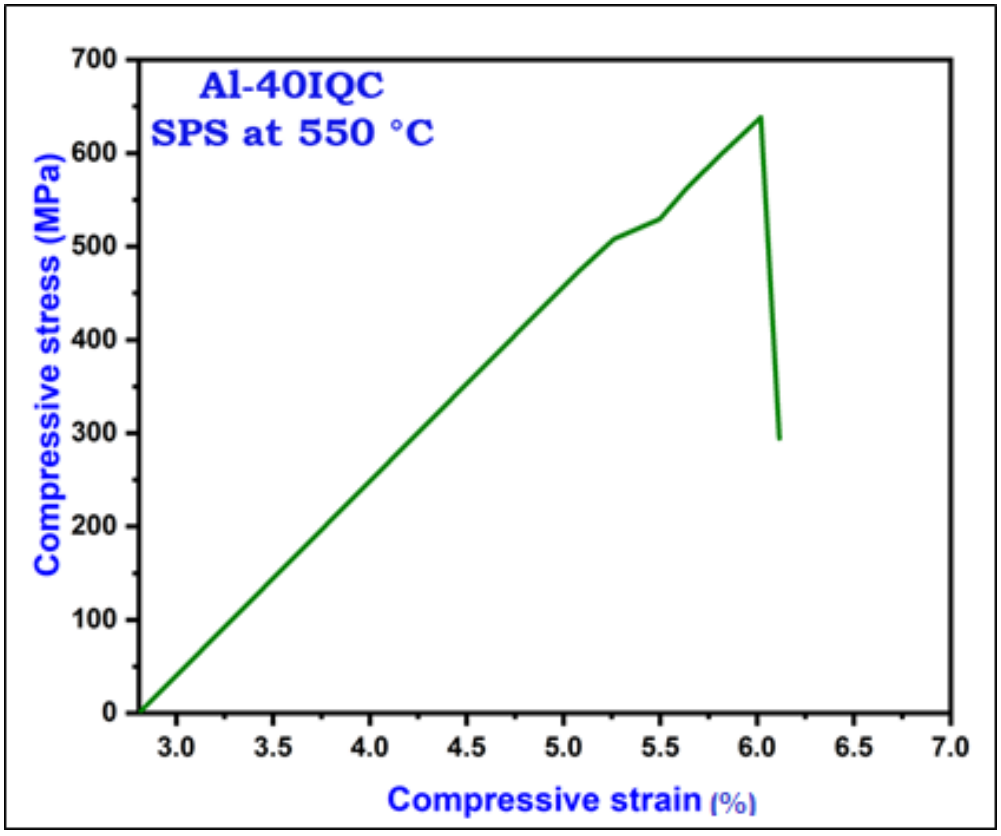

Figure 4. 19: Engineering compressive stress – strain diagram of Al-40IQC SPSed at 550 ℃ (823 K).

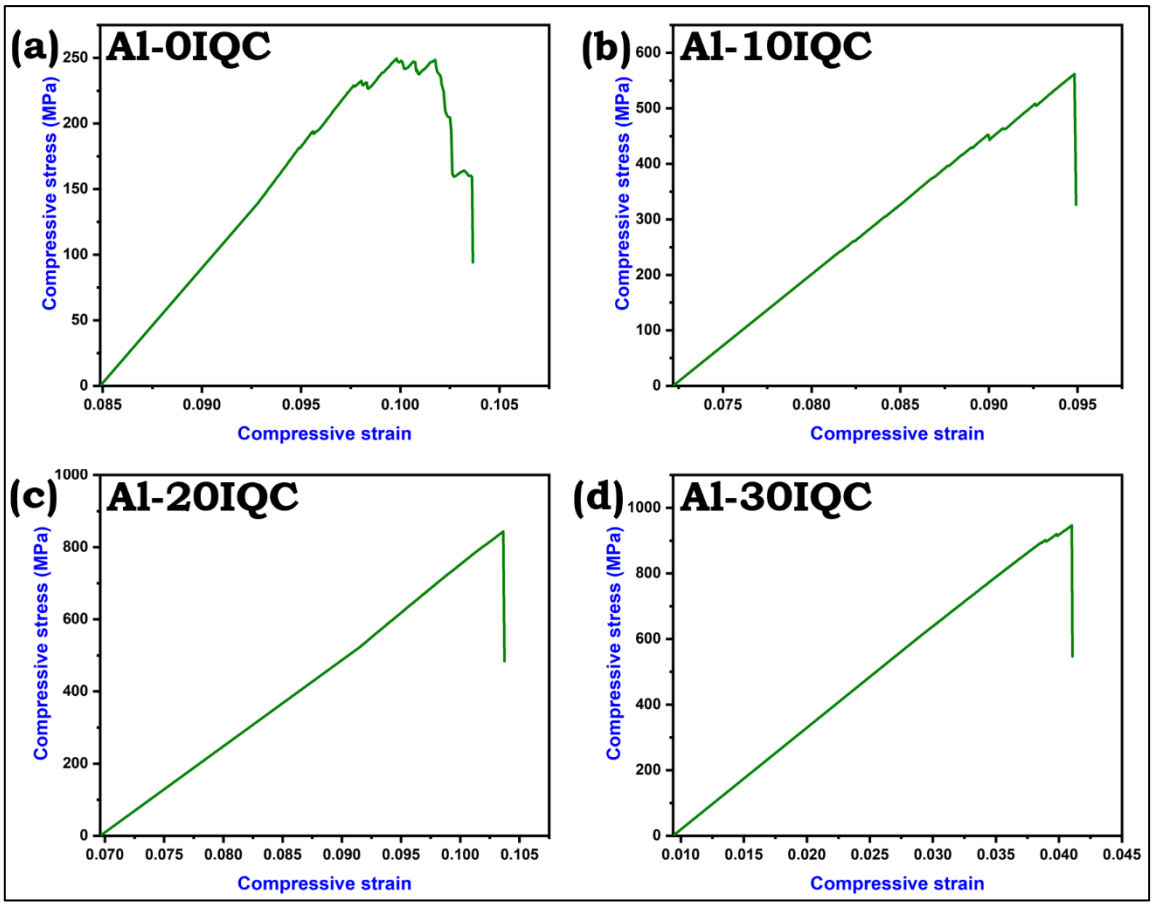

Figure 4. 20: Engineering compressive stress – strain diagram of (a) Al-0IQC, (b) Al-10IQC, (c) Al-20IQC, (d) Al-30IQC composite SPSed at 300 ℃ (573 K) with a pressure of 500 MPa.

The existence of face-centered order IQC phase even after SPS at 450 ℃ (723 K), and 550 ℃ (823 K) were still evident, confirming the hybrid nature of AMCs. Increasing the SPS temperature decreases the phase fraction of the IQC phase in the Al matrix. Also, the phase fraction of ω-Al_7Cu_2Fe crystalline phase increases for Al-40IQC SPSed at 550 ℃ (~48%) in contrast to 450 ℃ (~36%), as evident from its peak intensity (Figure 4.13 (a & b)). All the major diffraction peaks corresponding to λ and ω-phase may be seen in the powder XRD pattern of Figure 4.13 (a & b). The TEM micrograph of Al-40IQC composite sample SPSed at 550℃ shown in Figure 4.13 (c & d) is in conformity with the XRD results of SPSed samples shown in Figure 4.13 (b). The uniform distribution of reinforcement

particles is seen in the Al matrix composite, as evident from Figure 4.13 (c). The existence of quasicrystalline phase in the SPSed Al-40IQC AMCs was evident from Figure 4.13 (a and b). However, Figure 4.13 (d), the selected area diffraction pattern is taken from the Al-ω phase interface, in which the diffraction spots closely matches with the ω and λ phases.

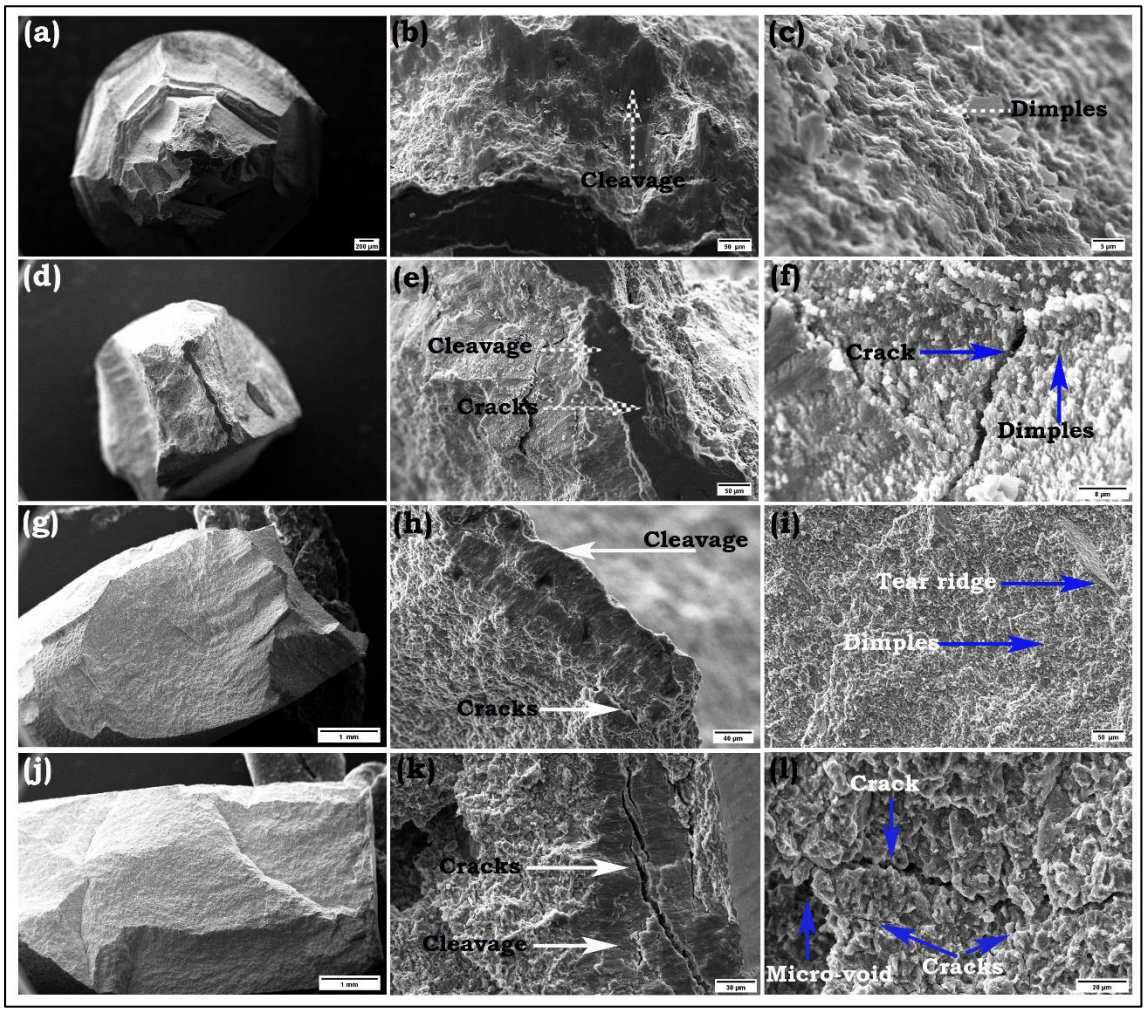

Figure 4. 21: Fractography of (a, b, c) Al-OIQC, (d, e, f) Al-10IQC, (g, h, i) Al-20IQC, (j, k, l) Al-30IQC SPSed at 300 ℃ (573 K) with a pressure of 500 MPa.

The back-scattered SEM micrograph of SPSed Al-40IQC composite is shown in Figure 4.14. The size, shape and uniform distribution of reinforcement particles in the Al matrix are quite evident from the SEM micrograph of Figure 4.14 (a) and (c) for Al-40IQC SPSed at 450 ℃ (723 K) and 550 ℃ (823 K) respectively. In the low magnification images,

the type of reinforcing phases is not so clear as it is intended to represent the statistical distribution of the reinforcements. From the SEM micrograph of Figure 4.14 (b & d), it is clear that the reinforcement particles have quasi-spherical, elongated and rod-like morphology after consolidation by SPS. The morphology of the various reinforcing phases is quite understood from the higher magnification SEM micrograph for Al-40IQC SPSed at 450 ℃ (723 K) and 550 ℃ (823 K) . Figure 4.14 (c) suggest three types of contrast, i.e. light grey, dark grey and black. The chemical composition corresponding to Spot-1, 2, 3 and 4 are mentioned in Table 4.2. As per Table 4.2, phase having the contrast of black, light grey and dark grey is having a nominal composition close to that of Al matrix, ω-phase and λ-phase respectively.

During sintering, due to diffusion of Cu, Al matrix is enriched with Cu concentration. In Al-40IQC composite SPSed at 450 ℃, the λ-phase and ω-phase are uniformly distributed in the Al matrix having dark grey and light grey contrast respectively. Similarly, back-scattered SEM micrograph of Figure 4.14 (d) represents mainly two types of contrast, i.e. black and light grey. The chemical composition corresponding to Spot-1, 2 and 3 marked in Figure 4.14 (d) are mentioned in Table 4.2. As per the chemical composition of the EDS spot mentioned in Table 4.2, corresponding to Al-40IQC composite SPSed at 550℃, phase having black and light grey contrast is having a nominal composition close to that of Al matrix and ω-phase respectively. As per the contrast of the phases, the volume fraction of dark grey and light grey phases in AMC SPSed at 450℃ was found to be ~49% and ~51% respectively. Similarly, the volume fraction of the dark grey and light grey phases in AMCs SPSed at 550℃ was found to be ~33% and ~67% respectively. It is further observed that the volume fraction of IQC+crystalline reinforcement increases to ~49% and ~56% from initial volume fraction of 40% for IQC in

Al-40IQC NC powder, due to interfacial reaction during SPS at 450℃ and 550℃ respectively. Furthermore, it is observed that the concentration of Cu in the Al matrix is more in comparison of NC powder SPSed at 450℃.

The SEM-EDS elemental map of Al-40IQC composite SPSed at 450 ℃ and 550 ℃ is represented in Figure 4.15 and 4.16, respectively. Figure 4.15 represents the SEM-EDS elemental map of Al, Fe, Cu, Mg and Si at the interface of the Al matrix and ω-phase reinforcement having rod-like or elongated type morphology. At the interface of the Al matrix and ω-phase, particles with three different contrast are distinctly seen. During SPS, due to diffusion of Cu into the Al matrix led to the formation of θ-Al_2Cu intermetallic phase at the interface. This is in conformity with the elemental overlay of individual elements at the interface. The Al is uniformly distributed in matrix, reinforcement and at the interface. Further, it was also observed that after consolidation Mg and Si were homogenously distributed and there was not signature for the formation of Mg-Si intermetallics precipitates.

Table 4. 3: Physical and mechanical property of SPSed Al-40IQC matrix composite.

SPS Temperature (˚C)	450	550
Density (as per rule of mixture) $g.cm^{-3}$	3.292	
Density (Experimental) $g.cm^{-3}$	2.921	3.267
Relative density (%)	88.69	99.23
Porosity (%)	11.31	0.77
Young's Modulus, E (MPa)	102	135
Compressive Yield Strength (MPa)	-	519
Ultimate compressive Strength (MPa)	-	639
Failure strain, ϵ_f (%)	-	~6

Table 4. 4: Physical and mechanical property of Al-IQC matrix composite SPSed at 300 ℃ (573 K) with a pressure of 500 MPa.

Sample designation	Density			Compressive strength		
	ρ_{exp} (g.cm^{-3})	ρ_{the} (g.cm^{-3})	Relative density (%)	Yield strength (MPa)	Ultimate strength (MPa)	Failure Strain (%)
Al-0IQC	2.50	2.70	92.90	241	249	~10%
Al-10IQC	2.69	2.83	95.05	525	561	~9%
Al-20IQC	2.94	2.97	98.90	799	843	~10%
Al-30IQC	3.08	3.11	99.12	910	946	~4%

The region belonging to reinforcement is enriched in Fe and deficit in Cu as evident from Figure 4.15. However, the region belonging to the interface of the Al matrix and ω-phase is rich in Cu and lean in Fe, establishing the presence of θ-Al_2Cu. This result is in conformity with the phase analysis done through XRD, as shown in Figure 4.12 (a). Figure 4.16 represents the SEM-EDS elemental map of Al, Fe, Cu, Mg and Si at the interface of the Al matrix and ω-phase reinforcement for Al-40IQC composite SPSed at 550 ℃. The Al is seen to be uniformly distributed in the matrix as well as reinforcement. However, the Fe and Cu are found to be rich in reinforcement and at the interface, respectively.

However, the phase evolved, microstructural features and mechanical properties changed by altering the processing condition of Al-IQC AMCs through SPS at 300 ℃ (573 K) with a pressure of 500 MPa. In this case it was observed that the IQC phase in the Al-IQC composite retains its identity even after SPS for 30 min. The reinforcement particles after SPS at 300 ℃ contains IQC phase as the major phase with minor fraction corresponding to the Al_2Cu and Al_7Cu_2Fe crystalline phases as discerned from the Figure

4.17 (a). Further from Figure 4.17 (b) it is observed that the major IQC phase co-exist with minor ω and θ phases. In the case of Al-IQC SPSed at 300 ℃ (573 K) no distinguishable contrast corresponding to the ω and θ phases was observed in Figure 4.18. However, due to low temperature SPS the particles size of IQC reinforcement particles are ~1.0 to 1.5 μm.

The interfacial reaction at the interfaces of the Al matrix and ω-phase leads to the formation θ-phase at the interface. The hybridization of these composite due to interfacial reaction during spark plasma sintering enhances the mechanical properties of these composite. The engineering compressive stress-strain diagram of Al-40IQC composite are shown in the Figure 4.19 and the physical and mechanical properties of Al-40IQC composite samples are mentioned in Table 4.3. From Table 4.3, it is quite evident that Young's modulus 'E' and compressive yield strength increases considerably after consolidation by SPS of these samples. The compressive yield strength and ultimate strength of Al-40IQC composite are reported to be 519 and 639 MPa, respectively.

This small size reinforcement particle and its homogenous distribution in Al matrix in Al-IQC composite SPSed at 300℃, helps to strengthen it to great extent as can be discerned from the engineering compressive stress–strain diagram of Figure 4.20. It was observed that by altering the processing parameters a hybrid Al-IQC composite can be fabricated with a strength ~900 MPa with a failure strain of ~5 to 10% depending upon the volume fraction of reinforcement. The fractograph of Al-IQC composite can be observed in the Figure 4.21. It can be seen that the Al-IQC composite fails by mixed mode of failure. The signature of dimple and cleavage fracture were quite prominent in Al-IQC fracture surfaces. However, on increasing the volume fraction of IQC, the cleavage fracture becomes more prevalent.

The various features observed are also marked on the individual fractograph shown in the Figure 4.21. The physical and mechanical properties of Al-IQC nanocomposite are reported in the Table 4.4. It was illustrated that with increasing the volume fraction of IQC in Al matrix the relative density increase ~99.1%.

4.4 Discussion

The present study addresses the exploitation of Al-Cu-Fe IQC as a potential reinforcement material for Al matrix to be used as a structural engineering material. The Al-Cu-Fe IQC alloys are known to be having very high hardness, corrosion resistance, low coefficient of friction and high wear resistance etc. [60]. These Al-Cu-Fe IQC reinforcements are used to engineer the interfaces of Al-matrix and IQC particles. In the past, many researchers had made considerable efforts in studying the microstructure and mechanical properties of Al-Cu-Fe IQC particles in pure Al matrix through melting and solidification routes [288,383,384]. For overcoming the problem associated with casting, i.e. porosity and homogenous distribution of reinforcement, few researchers had investigated the effect of MM and consolidation by hot pressing on microstructure and mechanical properties of Al/ Al-Cu-Fe composite [221,316,382,385–390]. It is of paramount importance to study the effect of IQC particles on microstructural refinement during MM and interfaces of these Al-IQC composite after SPS.

4.4.1 Structural and microstructural features of Al-IQC milled powder

The repetitive multidirectional collision during MM leads to increase stress at high strain rates with an increase in the dislocation density. In the course of the random collision of the Al matrix and IQC particles in between balls and vial wall during MM, the coarse-grained Al matrix particles undergo fragmentation and get nanostructured. The average crystallite size, lattice strain and particle size of 6082 Al matrix depends upon the duration

of MM (Table 4.1 and Figure 4.6). The different stage of MM is also discussed in details by Suryanarayana [347] and Fetch [391] . Fetch has explained the microstructural refinement of materials during MM in five (5) different stage as (i) flattening during collision, (ii) cold welding, (iii) fracturing, (iv) equiaxed powder particle during random welding and (v) steady-state powder particle formation [391]. As explained by Fetch, during the steady-state powder particle formation, effective grain refinement and particle refinement also become steady. In the present investigation also, after 30 h of MM, the microstructural refinement is not as appreciable as before 30 h of MM (Figure 4.6 and Table 4.1). Further, Basariya et al. made considerable efforts to study the effect of unconventional reinforcement like a hard garnet particle and CNTs on the variation of crystallite size and particles size as a function MM duration [238,392,393]. They have also reported saturation in the grain refinement and particle size after MM of Al-based composite for 30 h of MM. They have reported the refinement of 6082 Al matrix after 50 h of MM is ~ 36 nm and lattice strain ~0.3689%. The level of microstructural refinement is also dependent on the crystal structure of powder particles subjected to MM. The intensity of refinement is less in comparison to brittle intermetallic as described by Suryanarayana and Fetch [347,391]. In the present investigation, the embedded hard quasicrystalline Al-Cu-Fe IQC particles were responsible for considerable grain refinement of 6082 Al matrix (~16 nm) after 50 h.

Mukhopadhyay et al. [375,394,395] have described the order-disorder transformation of face-centred IQC phase is dependent on the strain-induced during MM. The mechanism of MM in the present investigation is mostly ductile-brittle type as described by a few researchers and co-workers. Therefore, even after MM of Al-Cu-Fe IQC particle reinforced Al matrix for 50 h, the ordered face-centred IQC phase is able to retain

its identity. The (311111) ordered reflection of IQC in Al-40IQC even after 50 h, establishes the fact that the threshold strain required for disordering of IQC phase is not achieved in the present study as described by Mukhopadhyay and co-workers [375,394,395]. The ballistic jump of atoms during the MM is responsible for structural transformation of many complex intermetallics and quasicrystalline materials [375,394–397]. Although, the increased volume fraction of IQC particles in 6082 Al matrix, help is achieving considerable crystallite and particle size refinement, however in due course, the IQC phase partially transforms to $Al_{13}Fe_4$. In the previous investigation carried by Mukhopadhyay et al. [395,398] and Tiwari et al. [377], has suggested the structural transformation of Al-Cu-Fe IQC phase to approximant phases. The transformation of this IQC phase to approximant phases is either strain-induced transformation or due to fluctuation in the chemical composition. The transformation of IQC to $Al_{13}Fe_4$ phase is explained by Cheng et al., by a combination of linear space and projection strip rotation leading to special linear phason strain [376]. A similar transformation of Al-Cu-Fe IQC phase is also observed by Mukhopadhyay et al., during MM of IQC phase (with minor crystalline phase in the as-cast and annealed samples) [377]. In the present investigation, the MM is carried in WC vials with WC balls. Therefore, the chances of contamination from milling media may be ruled out. However, due to the straining and ballistic diffusion of Al atoms from the Al-matrix to IQC phase, maybe collectively responsible for its transformation. This ballistic diffusion of Al atoms into the IQC phase locally transforms the IQC phase to $Al_{13}Fe_4$ phase.

4.4.2 Mechanical property and interfacial strengthening of composite

In the present investigation, considerable efforts were made to investigate the interfaces and its effect on the mechanical properties of age-hardened 6082 Al matrix composite reinforced with Al-Cu-Fe IQC particles through SPS. In the present investigation, during sintering, IQC particles transform to ω-Al_7Cu_2Fe phase. Increasing the SPS temperature from 450 ℃ (723 K), and 550 ℃ (823 K) leads to an increase of the phase fraction of ω-phase in comparison to λ-phase. In the temperature range of 400 ℃ to 600 ℃, ω-phase is found to be stable, as reported by Salimon et al. [399]. Previously, a few researchers have made efforts to investigate the microstructure and mechanical properties of Al/Al-Cu-Fe composite prepared by powder metallurgical processing. However, MM was only used for a homogenous distribution of IQC particles in the matrix regardless of the microstructural refinement of these NC powder for a very short duration. Therefore, the $Al_{13}Fe_4$ particles present in the Al-40IQC composite after SPS is the result of MM upto 50 h. The presence of the intermetallic phase, i.e. λ-phase, θ-phase, ω-phase along with IQC phase helps for enhancing the mechanical properties of these composites. Further, the diffusion of Cu into the 6082 Al matrix has an additional effect of solid solution strengthening. In a recent investigation by Dobrzyńska et al.[300] has incorporated gas atomized IQC particles with B2-type Al (Cu, Fe) phase into the Al matrix and the same consolidated by hot pressing at 400 ℃ (673 K). For Al matrix with 40 and 60 vol% of IQC particles, the compressive yield strength was reported to be 200 MPa and 370 MPa respectively. The enhanced compressive yield strength of the Al matrix with 60 vol% of IQC was suggested due to formation Al_2Cu intermetallic at the interface of IQC and Al matrix. The strengthening of the metal matrix composite is dependent on direct as well as indirect factors. The direct strengthening is due to the reinforcement particles present in the matrix, which transfers the load to the reinforcement during loading. The indirect

strengthening of these composite is due to solid solution strengthening and precipitation strengthening. In the present investigation, compressive yield strength and ultimate strength of Al-40IQC composite SPSed at 550 ℃ (823 K) is 519 MPa and 639 MPa respectively. This high compressive yield strength and ultimate strength is due to both direct and indirect strengthening in present investigation. The existence of IQC and λ-$Al_{13}Fe_4$ phase during MM, and formation of ω-Al_7Cu_2Fe and Al_2Cu phases during SPS in age-hardenable 6082 Al matrix is responsible for direct strengthening. The self-diffusion coefficient of Cu in more than that of the Fe. Therefore, during fabrication of Al-40IQC composite through SPS, diffusion of Cu takes place into the Al-matrix. The solid solution of Al(Cu) is evident from Table 4.2 and Figure (4.14, 4.15, 4.16) and is responsible for the indirect strengthening of these composites. Joseph et al. [400] have recently described the effect of direct strengthening and indirect strengthening on the mechanical properties of the Al-ω composite processed through SPS. They have also observed the formation of Al_2Cu precipitates in the Al(Cu) solid solution strengthened matrix. In the present investigation due to existence of λ-phase and IQC phase along with ω and θ phase in the solid solution strengthened 6082 Al matrix, the compressive yield strength is significantly higher than the Al-IQC composite previously reported in the literature. Although, during sintering, a considerable fraction of the IQC phase transforms to its crystalline phases but not entirely. During SPS for the shorter duration, the minor fraction of the IQC phase was retained along with the formation of other crystalline approximant phases due to the interfacial reaction between the IQC phase and the Al matrix. This has led to the formation of hybrid composite with QC as well as intermetallic reinforcements.

In an investigation, El Kabir et al. [401] fabricated the AMCs reinforced with IQC alloy by hot isostatic pressing (HIP) at 823 K and 180 MPa for 2 h. They have reported the

transformation of IQC phase to ω-phase and further studied its strength at an elevated temperature (293 K – 773 K). The strength of these kind of AMCs progressively decreases on increasing the temperature. Laplache et al. [326,382] extended the work of El kabir and fabricated AMCs by hot isostatic pressing at 673 K and 823 K. The processing of AMCs at 673 K was able to retain the structure of IQC phase, while HIP at 823 K leads to the complete transformation of IQC phase in AMCs to ω-phase. The ratio of yield strength and shear modulus ($\sigma_{0.2\%}/\mu$) of pure Al, Al-IQC and Al-ω composite shows dependence on the temperature with two distinct regime having a transition at ~573 K. The value of $\sigma_{0.2\%}/\mu$ decreases gradually upto 573 K, however a pronounced decrease was observed after this temperature range. The $\sigma_{0.2\%}/\mu$ value for Al-ω composite is almost two times more than Al-IQC composite at room temperature and the difference between them decrease gradually at elevated temperature. The $\sigma_{0.2\%}/\mu$ is almost same for Al-IQC and Al-ω composite from 573 K onwards. However, for the case of Al-IQC composite SPSed at high pressure a significant rise in the compressive yield strength was observed with failure strain comparable to that of the Al-40IQC SPSed composite. The rise in the strength and density as a function of volume fraction of reinforcement can be understood by the findings of Ghasali et al. [402]. The have explained the increase in the strength and density can be ascertained due to increase in the micro-sparking during high pressure and ultra low temperature SPS. Therefore, the Al-IQC composite SPSed at high pressure and moderate temperature yield hybrid AMCs with major IQC phase along with minor ω and θ-phase, and shows better compressive strength compared to that of the sintered at 550 °C.

Due to the chemical reactivity and formation of intermetallic phases at the interface of IQC and Al, the load transfer will be gradual, and it inhibits the formation of cracks at the interface due absence of stress concentration. However, in case of metal matrix

composite reinforced with ceramic reinforcement, weak interfacial bonding leads to the formation and propagation of cracks from the interface of the matrix and reinforcement due to stress concentration. The strong interfacial bonding in the Al-IQC AMCs with intermetallic phases at the interfaces are beneficial for structural applications. The interfaces in 6082 Al matrix composite reinforced with IQC particles may be engineered for designing AMCs having a high strength to weight ratio for potential application in the automobile sector.

4.5 Conclusions

The mechanical milling of 6082 Al matrix reinforced with varring volume fraction of IQC upto 50 h of MM, followed by fabrication through spark plasma sintering significantly enhances the compressive strength. The following can be concluded from the present investigation:

1. The structural transformation of the IQC phase in Al-40IQC NC powder (partially) to λ-$Al_{13}Fe_4$ phase subjected to MM for 50 h. The face-centred ordered reflection of IQC, i.e. (311111) could retain its identity even after 50 h of MM. However, no such structural transfomation was observed for Al-IQC NC powder reinforced upto 30 vol% of IQC reinforcement.
2. The MM process induces microstructural refinement as well as enhances the embedding of IQC particles in the Al matrix with good interfacial integrity.
3. The SPS of Al-40IQC AMCs at 450 ℃ (723 K), and 550 ℃ (823 K) leads the formation of ω-Al_7Cu_2Fe phase, Al_2Cu phase along with a minor fraction of pre-existing phases of IQC and $Al_{13}Fe_4$.
4. The direct and indirect strengthening in Al-40IQC SPSed AMCs significantly increases the compressive yield strength (~519 MPa) with appreciable failure strain

(~6 %). The interfacial reaction during SPS of these AMCs leads to hybridization of Al-40IQC AMCs.

5. The SPS of Al-IQC AMCs at 300 ℃ (573 K) and 500 MPa leads the retension of IQC phase along with minor fraction of ω-Al_7Cu_2Fe phase, Al_2Cu phase. The Al-IQC sintered at high pressure does not have any signature of $Al_{13}Fe_4$ as it was observed for Al-40IQC SPSed at 450 ℃ (723 K), and 550 ℃ (823 K)
6. The enormous increase in the compressive strength was observed for Al-IQC composite SPSed at 300 ℃ (573 K) and was ~900 MPa. This significant rise can be attributed to the retention of IQC phase along with the presence of minor crystalline phases.